BIOCHEMISTRY
including biophysical chemistry & molecular biology

Article

pubs.acs.org/biochemistry

Cysteine-Rich Positions Outside the Structural Zinc Motif of Human Papillomavirus E7 Provide Conformational Modulation and Suggest Functional Redox Roles

Lucía B. Chemes,[†,§] Gabriela Camporeale,[†,§] Ignacio E. Sánchez,[‡] Gonzalo de Prat-Gay,*[,†] and Leonardo G. Alonso*[,†]

[†]Protein Structure−Function and Engineering Laboratory, Fundación Instituto Leloir and IIBBA-CONICET, Av. Patricias Argentinas 435, 1405 Buenos Aires, Argentina

[‡]Protein Physiology Laboratory, Departamento de Quimica Biologica, Facultad de Ciencias Exactas y Naturales and IQUIBICEN-CONICET, Universidad de Buenos Aires, C1428EGA Buenos Aires, Argentina

Supporting Information

ABSTRACT: The E7 protein from high-risk human papillomavirus is essential for cell transformation in cervical, oropharyngeal, and other HPV-related cancers, mainly through the inactivation of the retinoblastoma (Rb) tumor suppressor. Its high cysteine content (~7%) and the observation that HPV-transformed cells are under oxidative stress prompted us to investigate the redox properties of the HPV16 E7 protein under biologically compatible oxidative conditions. The seven cysteines in HPV16 E7 remain reduced in conditions resembling the basal reduced state of a cell. However, under oxidative stress, a stable disulfide bridge forms between cysteines 59 and 68. Residue 59 has a protective effect on the other cysteines, and its mutation leads to an overall increase in the oxidation propensity of E7, including cysteine 24 central to the Rb binding motif. Gluthationylation of Cys 24 abolishes Rb binding, which is reversibly recovered upon reduction. Cysteines 59 and 68 are located 18.6 Å apart, and the formation of the disulfide bridge leads to a large structural rearrangement while retaining strong Zn association. These conformational and covalent changes are fully reversible upon restoration of the reductive environment. In addition, this is the first evidence of an interaction between the N-terminal intrinsically disordered and the C-terminal globular domains, known to be highly and separately conserved among human papillomaviruses. The significant conservation of such noncanonical cysteines in HPV E7 proteins leads us to propose a functional redox activity. Such an activity adds to the previously discovered chaperone activity of E7 and supports the picture of a moonlighting pathological role of this paradigmatic viral oncoprotein.

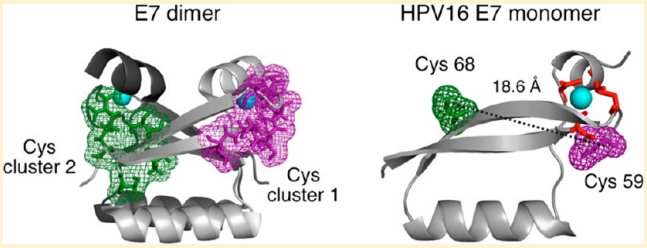

Human papillomaviruses (HPV) have drawn the attention of the scientific community since the discovery of their direct involvement in human cancer development.[1,2] Over 100 papillomavirus types that infect humans have been described,[3] only a subset of which possess oncogenic potential and have been classified as "high-risk" types.[2] As opposed to high risk HPVs, many HPV types produce benign lesions and are classified as "low risk".[2] Moreover, most HPV infections are self-limited and resolve without clinical manifestation.[4] In fact, HPV-induced neoplastic lesions do not produce infective particles and can be considered as unproductive events in the HPV life cycle.[5]

In order to produce infective particles, the HPV genome must replicate within a stratified epithelium, and as HPVs are devoid of the enzymatic machinery required to duplicate their genome, these viruses must use the host DNA replication machinery to generate new infective viruses.[6] Most papillomaviruses infect basal undifferentiated cells of stratified skin and mucous epithelia, where the genome is initially amplified and maintained at low copy number, but subsequent viral replication takes place in differentiating keratinocytes, which have withdrawn from the cell cycle. The HPV genome codes for a handful of proteins that act in a coordinate manner to override the control mechanisms that strictly regulate the host cell cycle.[7] This complex task depends largely on the E7 oncoprotein, which is essential for stimulating S-phase reentry in differentiating keratinocytes, producing an uncoupling of proliferation and differentiation in these cells.[8] According to the experimental evidence obtained from the prototypical E7 protein from the HPV16 type (HPV16 E7), E7-related functions are mediated by its ability to interact with multiple cellular targets.[9,10] The retinoblastoma protein (Rb) was the first cellular target identified for the E7 protein.[11] High affinity binding of E7 to Rb is required for the transforming properties of the high-risk HPV16 E7 protein in transfected cells,[12] and it is the primary and best-characterized interaction related to HPV-mediated cellular transformation.[13] Rb binding is a property shared by both high- and low-risk HPVs.[14] Persistent

Received: November 21, 2013
Revised: February 5, 2014
Published: February 21, 2014

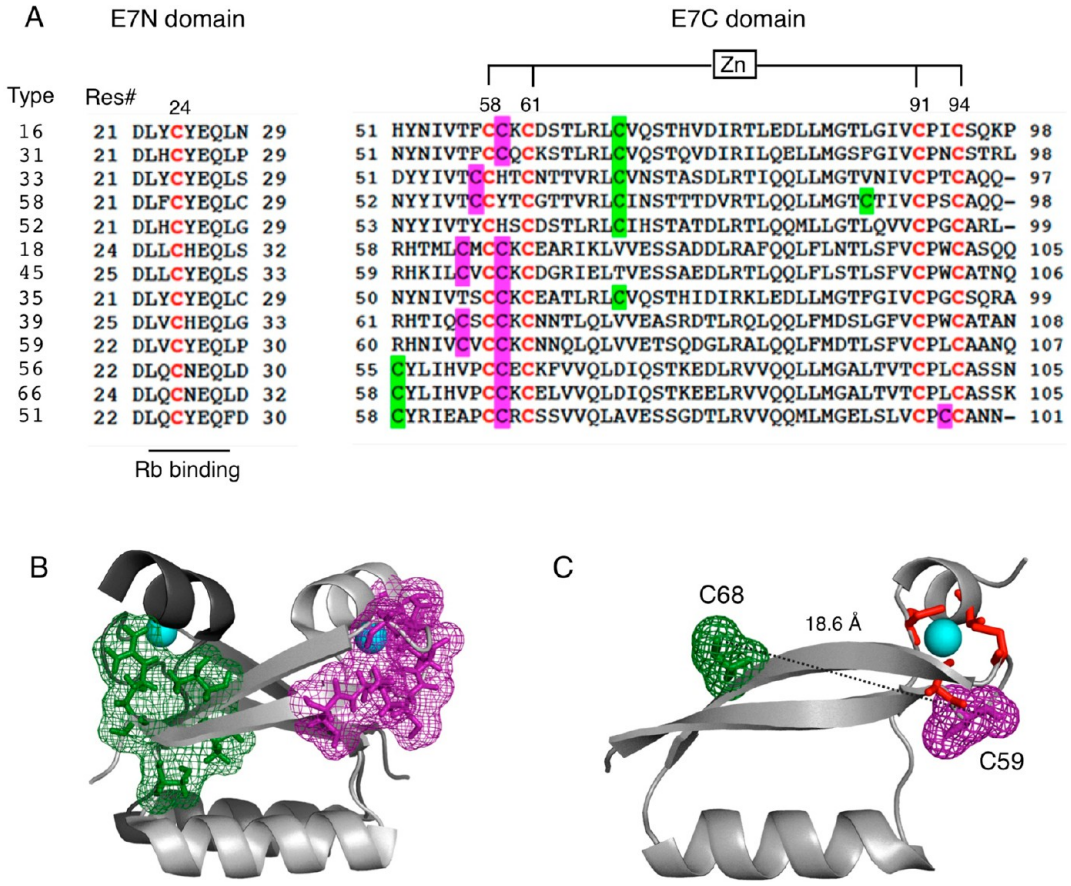

Figure 1. Distribution of cysteine-rich positions in the E7 oncoprotein. (A) Alignment of 13 high-risk E7 sequences. A portion of the E7N and the entire E7C domains are shown. Canonical cysteine residues involved in Rb binding and Zn coordination are shown in red, while noncanonical cysteines located in Cluster 1 and Cluster 2 regions in E7C are indicated in pink and green, respectively. The 10 Cys-rich positions previously identified in 219 papillomavirus E7C sequences[25] are indicated below the alignment; pink circles: Cluster 1 positions; green circles: Cluster 2 positions. (B) Structure of the HPV45 E7 dimer (PDB id: 2F8B) showing the location of Cluster 1 (pink sticks) and Cluster 2 (green sticks) Cys-rich positions in one E7 monomer. Cyan shperes: Zn atoms. Each monomer in the homodimer is represented in light and dark gray, respectively. Cluster 1 positions are close to the Zn coordination site of the same monomer, while Cluster 2 positions are close in space to the Zn coordination site of the opposite monomer. (C) Model structure of the HPV16 E7 monomer obtained using Modeler and the HPV45 E7 monomer as a template (PDB id: 2EWL) (see Materials and Methods). Cyan sphere: Zn atom; red sticks: Zn-coordinating cysteines; pink sticks: noncanonical cysteine 59 residue; green sticks: noncanonical cysteine 68 residue. The distance between the -SH groups of cysteines 59 and 68 is indicated.

expression of the HPV16 E7 protein is required for maintenance of the transformed phenotype.[15] It has been described that HPV16-positive cervical cancer lesions show a higher oxidative environment than normal noninfected tissues and a marked down-regulation of antioxidant enzymes such as superoxide dismutase, catalase, and glutathione peroxidase.[16−18] Moreover, it was shown that the sole expression of HPV16 E7 in HaCaT keratinocytes induces oxidative stress.[19]

HPV16 E7 is a small acidic 98-amino-acid protein[20] with two distinct structural domains, the globular C-terminal domain (E7C) for which X-ray and NMR structures have been solved for HPV types 1 and 45[21,22] and the intrinsically disordered N-terminal domain (E7N IDD), which is extended in solution and lacks canonical secondary and tertiary structure elements.[23] Although high-resolution structures show a homodimeric arrangement for the E7C domain,[22] E7 shows a complex hydrodynamic behavior in solution and exhibits multiple monomerization−dimerization−oligomerization equilibria with a reported dimer dissociation constant of ∼1 μM.[24] HPV16 E7 presents seven cysteine residues in its sequence, five of which have a strict or very high conservation degree across HPVs[25] (Figure 1A). HPV16 E7 binds one Zn atom per monomer through a tetra-cysteine coordination site located in the globular E7C domain[26] (Figure 1A). Metal coordination is essential for maintaining the structural integrity of the protein, and metal loss leads to the formation of large spherical soluble oligomers (E7SOs).[27] The four cysteine positions corresponding to the tetra-cysteine Zn binding motif, CxxC-29aa-CxxC (positions 58, 61, 91, and 94 in the HPV16 E7 sequence) are strictly conserved across human and animal papillomavirus types.[25] A fifth highly conserved cysteine residue (85% occurrence) corresponds to position 24 in the HPV16 E7 sequence and is located in the IDD E7N domain within a short linear motif responsible for Rb binding that spans residues 21−29 (DLYCYEQLN)[25] (Figure 1A). A quantitative investigation of the interaction mechanism between the HPV16 E7 protein and the RbAB domain in solution revealed that 90% of the binding energy is provided by the LxCxE motif, with an additional binding determinant located in the E7C domain, establishing a dual-contact mode.[28] Cysteine 24 in HPV16 E7 is located in the IDD domain and hence is highly exposed to the solvent and to oxidative agents, which are present in dysplastic and neoplastic tissues that are under oxidative stress.[16] The redox regulation of this fundamental cysteine and

dx.doi.org/10.1021/bi401562e | *Biochemistry* 2014, 53, 1680−1696

the consequences of its oxidation on Rb binding remain unknown so far.

On the basis of its high cysteine content, HPV16 E7 can be considered as a cysteine-rich protein, with seven out of 98 residues (~7%) corresponding to this amino acid, a proportion well above the overall average content for mammalian proteins (2.3%[29]). Recently, a detailed study on the sequence evolution of the globular homodimeric E7C domain based on the alignment of 219 papillomavirus sequences led us to identify 10 cysteine-rich positions within the E7 sequence in addition to the canonical cysteines involved in Zn and Rb binding. Despite presenting fairly low degrees of conservation, these noncanonical positions exhibit at least 5.9% cysteine abundance, 4-fold above the average percentage reported in UniProt (Figure 1A).[25] About 70% of E7 sequences possess at least one noncanonical cysteine occupying one of these ten positions, and 30% of E7 sequences present two noncanonical cysteines.[25] These noncanonical cysteine-rich positions can be classified in two clusters that differ in their relative orientation with respect to the Zn binding sites of each monomer.[25] Cluster 1 positions (residues 56, 57, 59, 60, 63, and 98 of the HPV16 E7 sequence) are close in sequence to the Zn binding site of the same monomer, while Cluster 2 positions (residues 51, 68, 69, and 71 in HPV16 E7) are distant in sequence from the Zn binding site of the same monomer but are spatially proximal to the Zn binding site of the second monomer in the structure of the E7 dimer (Figure 1B). HPV16 E7 presents two noncanonical extra cysteines in addition to those involved in Zn and Rb binding, located at positions 59 (Cluster 1, magenta) and 68 (Cluster 2, green) (Figure 1C).[25] Strong epidemiological evidence indicates that 13 papillomavirus types (HPV types 31, 33, 35, 39, 45, 51, 52, 56, 58, 59, and 66) are considered high risk for the development of cervical cancer and therefore are considered of clinical relevance.[30] With the exception of HPV 52, all E7 proteins from this group of high-risk types contain at least two noncanonical cysteines in their sequence (Figure 1A).

The importance of the cysteine residue is based on its particular chemical behavior, due to the presence of the ionizable thiol group, which is an excellent nucleophile at neutral pH.[31,32] This reactivity makes cysteine a likely target for chemical redox modifications that often lead to redox-regulation of protein function.[33−35] Cysteine can suffer many chemical modifications that include reversible changes such as the formation of disulfide bridges, glutathionylation,[36,37] and sulfenic acid formation,[34] as well as often irreversible changes such as sulfinic and sulfonic acid formation.[38,39] The oxidation agent and redox potentials that trigger cysteine modification within the cell are finely tuned and depend largely on the structural context of the reactive cysteines.[40] As an example, while the equilibrium oxidation constant for the formation of an intramolecular disulfide bridge between adjacent cysteines present in the CXXC motif of folded thiorredoxin is 10^{-16} M,[41] the equilibrium oxidation constant for formation of an intramolecular disulfide bridge in the urea-unfolded thiorredoxin is 0.026 M.[41]

The reactivity of the thiol group and the high prevalence of noncanonical cysteines in E7 proteins from clinically relevant HPV strains, together with the fact that HPV transformed tissues own high levels of oxidative stress, suggest a previously undescribed functional role for the noncanonical cysteines present within the E7 sequence. In the present work, we assessed the redox regulation and chemical reactivity of cysteines in the high-risk HPV16 E7 protein and their consequences on E7 structure and conformation, by using a combination of protein mutagenesis, spectroscopy, and mass spectrometry techniques.

MATERIALS AND METHODS

Protein Expression and Purification and Peptide Synthesis. The E7 wild type protein from the HPV 16 strain was obtained as described earlier.[20] Briefly, HPV 16 E7 was cloned as a thrombin-cleavable fusion protein downstream of the maltose binding protein (MBP) in a p-MALc2 vector (New England Biolabs) and expressed in the *E. coli* TB1 strain. After cleavage of the MBP-E7 fusion protein with protease, the isolated E7 protein was obtained containing two extra amino acids (glycine and serine) at the amino terminus due to the engineered thrombin cleavage site. The HPV 16 E7 protein was also cloned into a PTZ18u vector under the T7 promoter downstream to a short peptide (19 aa) of the β-galactosidase protein. An enterokinase (EK) cleavage site with the sequence DDDDK was inserted between the peptide and the amino terminus of the E7 protein. The cysteine mutants on the E7 HPV16 protein were obtained by site-directed, inverse polymerase chain reaction mutagenesis of the PTZ18u E7 HPV16 plasmid, used as a template. For this purpose, primers were synthesized containing the desired cysteine to alanine substitution (Integrated DNA Technologies). The obtained PCR fragment containing the mutation was ligated, and the resulting plasmid was sequenced in order to confirm the desired mutation and then transformed into BL21(DE3) *E. coli* strain for expression. By using the EK protease we obtained the E7 mutant proteins with the free N-terminus without the addition of any extra amino acid. Inclusion bodies (IBs) containing HPV-16 E7 mutants were purified as described.[27] The final step in the purification of E7 wild type and mutant proteins is always a size exclusion chromatography in a Superdex 75 column (GE Healthcare Bio-Sciences Corp, USA) that is performed in 10 mM sodium phosphate, pH 7.0 buffer without the addition of any reductant agent (DTT or 2-mercaptoethanol would interfere in subsequent analytical determinations of the protein oxidation state). Concentrated stock proteins without the addition of any reductant were maintained at −80 °C during 3 months without any appreciable oxidative damage of the sample. The expression and purity of the purified proteins were checked by 15% SDS-PAGE Coomassie blue stained.[42] All proteins presented 90% purity and no more than 10% of oxidized dimeric species. To obtain oxidized E7desLxCxE, a solution containing 50 μM of protein in 10 mM potassium phosphate buffer and 5 mM total glutathione concentration with a GSH/GSSG ratio of 0.1, pH 7.5, was incubated 80 min at 37C. After confirming by RP-HPLC that the oxidized species reached not less than 78%, the sample was desalted in a PD-10 column (GE Healthcare Bio-Sciences Corp, USA) equilibrated with 10 mM potassium phosphate buffer, pH 7.5. Oxidized E7desLxCxE protein was concentrated up to 20 μM and stored at −80 C.

The N-terminal peptide spanning the first 40 amino acids of the E7 HPV16, which includes the cysteine 24, was obtained by chemical synthesis at the W. M. Keck Facility (Yale University, New Haven, CT) with the N-terminal acetylated and C-terminal amidation.

Colorimetric Determination of Zn and Thiol Titration. Zinc release by thiol titration was determined spectrophotometrically by the measurement of the metallochromic indicator PAR.[43] Purified E7 wild type protein at a concentration of 5 μM was incubated with PAR (100 μM) in 50 mM potassium phosphate buffer, pH 7.5 at RT. Under this condition, only soft-bound metal or adventitious metal is determined because the constant affinity for Zn of the E7 protein is higher than the PAR-

Zn constant affinity and structural tetrahedrally coordinated Zn is not transferred to PAR. By adding quantified aliquots of the organomercury agent PMPS, which readily reacts with sulfhydryls in proteins, Zn is released from E7 protein, and the reaction was monitored at 500 nm. The exact metal content was determined from a calibration curve using a Zn standard solution (Sigma, St Louis, MO).

Thiol titration was performed by adding successive quantified aliquots of PMPS to a 5 μM E7 wild type protein in 50 mM potassium phosphate buffer, pH 7.5 at RT. The reaction of PMPS with the thiol group of cysteines is followed at 250 nm.

The Zn content of E7 mutants was evaluated by adding PMPS to a final concentration of 100 μM to a sample containing 3 μM concentration of each protein and 100 μM PAR in 50 mM potassium phosphate buffer, pH 7.5. The formation of PAR-Zn complexes was assessed by following the time trace at 500 nm. The addition of an excess of DTT (250 μM final concentration) displaces the PMPS from the protein (DTT provides an excess of reactive thiol groups) and allows the protein to reup take Zn. Due to the high affinity of the E7 proteins for Zn, the addition of DTT leads to a decrease in the absorbance at 500 nm (i.e., the PAR-Zn complexes are dissolved).

Quantitative Thiol Determination by DTNB. A sample containing 3 μM protein in 50 mM phosphate buffer pH 7.5 and 0.25 mM DTNB was incubated for 5−10 min, and the absorbance at 412 nm was obtained.[44] A calibration curve was done using reduced glutathione (GSH) as standard.

Determination of Redox Equilibria in Glutathione Buffer and H_2O_2 Oxidation. The redox equilibria of the E7 wild type and cysteine mutants was assessed by incubating a protein solution with different reduced and oxidized glutathione ratios (N), where N is [GSH]/[GSSG] at a constant total glutathione concentration. For each evaluated protein, a curve was obtained by incubating 250 μL of a solution containing 15 μM E7, 5 mM final glutathione concentration with different N ratio in 50 mM potassium phosphate buffer, pH 7.5 at 8 C overnight (18 h). To stop redox reaction, 200 μL of GdmCl 6.0 M and 0.1% TFA were added to E7 samples. The identification of the oxidized species and the quantitative analysis of the reduced and oxidized species in E7 wild type and cysteine mutants were performed by reverse phase HPLC (RP-HPLC) using a C_4 column, 250 mm × 4.6 mm (Bio-Basic-C4, Thermo Scientific, PA, USA). The eluted species were detected at 220 nm using an isocratic step at 20% (v/v) acetonitrile/water 0.1% TFA for 10 min and a gradient step from 20% to 70% (v/v) acetonitrile/water 0.1% TFA in 25 min. The oxidation of E7 wild type with hydrogen peroxide was performed by incubating 250 μL of a solution containing 15 μM E7 in 50 mM potassium phosphate buffer, pH 7.5 for 30 min at 37 °C with 150 μM of H_2O_2. The reaction was stopped by adding 200 μL of GdmCl 6.0 M, 0.1% TFA, and 5 mM methionine.

The analysis of the redox equilibrium in glutathione buffer of the N-terminal peptide (1−40) was performed using a different RP-HPLC method using a C_{18} column, 250 mm × 4.6 mm (Bio-Basic-C18, Thermo Scientific, PA, USA). The eluted species were detected at 220 nm by an isocratic step from 10% (v/v) acetonitrile/water 0.1% TFA for 10 min and a gradient step from 10% to 50% (v/v) acetonitrile/water 0.1% TFA in 30 min. The reduced fraction at each N ratio was calculated by integrating both the area under the peak corresponding to the reduced species and the total peak area (all peaks). The equilibrium constant (K_{mix}) for the formation of a mixed disulfide bridge between the cysteine 24 and the glutathione was calculated by fitting the reduced fraction to the following equation:

$$\mathrm{RF} = \left[\frac{1}{(K_{mix}/N) + 1}\right] + b \quad (1)$$

where RF is the reduced fraction, K_{mix} is the equilibrium constant for the reaction of disulfide formation between a protein cysteine (P(SH)) and glutathione according to the following equilibrium:

$$\mathrm{P(SH)} + \mathrm{GSSG} \leftrightarrow \mathrm{PSSG} + \mathrm{GSH}$$

N is the ratio between GSH and GSSG, and b is a constant that corrects for a protein population that is refractive to oxidation.

Intact Protein Analysis and Identification of Cysteine Connectivity by MALDI-TOF. MALDI-TOF mass spectrometry of intact protein was performed by diluting 1/5 v/v aliquots of the E7 samples in oversaturated solution of sinapinic acid in 30/70/0.1% (v/v) acetonitrile/water/TFA. A 1-μL aliquot of the sample was spotted onto a AnchorChip (Bruker, Billerica, MA, USA) and left to crystallize by air-drying. Samples were analyzed on a Bruker Microflex MALDI-TOF (Bruker, Billerica, MA, USA). Identification of cysteine connectivity in E7desLxCxE oxidized sample was performed by treating a protein solution (ca. 20−50 μM) with 56 mM iodoacetamide (IAA) in 50 mM Tris-HCl, pH 8.0 for 30 min at room temperature in a dark place in order to block reactive sulfhydryls. *N*-Ethylmaleimide (NEM) cysteine alkylation was performed by treating a protein solution (ca. 20−50 μM) with 30 mM NEM in 50 mM phosphate buffer, pH 8.0 for 30 min at room temperature in a dark place in order to block reactive sulfhydryls. The sample was precipitated by adding 10% v/v TCA on ice, and after centrifugation at 9000*g* for 30 min the supernatant was discarded and the sample was washed twice with cold acetone and left to dry. Pellet was resuspended with 50 mM Tris-HCl, 5 mM octyl β-D-glucopyranoside (OPG), pH 8.0 containing sequencing grade trypsin (Sigma, St Louis, MO) at 1/10 (w/w). When reductant was required, 5 mM concentration of ultrapure DTT was added to the reaction. Proteolysis was left to proceed for 18 h at 8 °C, and then the reaction was stopped by the addition of TFA to 0.1% final concentration. A 1-μL aliquot was spotted onto a AnchorChip (Bruker, Billerica, MA, USA), and 1 μL of oversaturated solution of α-cyano-4-hydroxycinnamic acid (HCCA) in 30/70/0.1% (v/v) acetonitrile/water/TFA was loaded to the protein sample. Samples were analyzed on a Bruker Microflex MALDI-TOF.

Binding of Reduced and Oxidized E7N to the RbAB Domain. Experiments were performed as described in ref 45. Briefly, the E7N peptide (1−2 mg) was labeled at its amino terminus with 1.5 mg/mL fluorescein isothiocyanate (FITC) in 100 mM sodium carbonate buffer, pH 8 for 2 h at room temperature and separated from labeling reagents by a desalting column (PD-10, GE Healthcare) followed by RP-HPLC. Oxidation of FITC-labeled E7N was performed as described, and the labeled and oxidized peptides were further purified by RP-HPLC. The purity of all preparations was evaluated by MALDI-TOF spectroscopy. Measurements were performed in a Jasco FP6500 fluorescence polarimeter assembled in L geometry, using excitation and emission wavelengths of 495 and 520 nm, with 3−5 nm bandwidth. All measurements were performed at 20 ± 0.1 °C in 20 mM sodium phosphate buffer, pH 7, 200 mM NaCl, and 0.1% Tween-20. For titration, increasing amounts of a concentrated solution of RbAB protein were added to a cuvette containing 100 nM FITC-labeled E7N peptide. Only for testing binding of reduced E7N to RbAB, 2 mM DTT was added to the

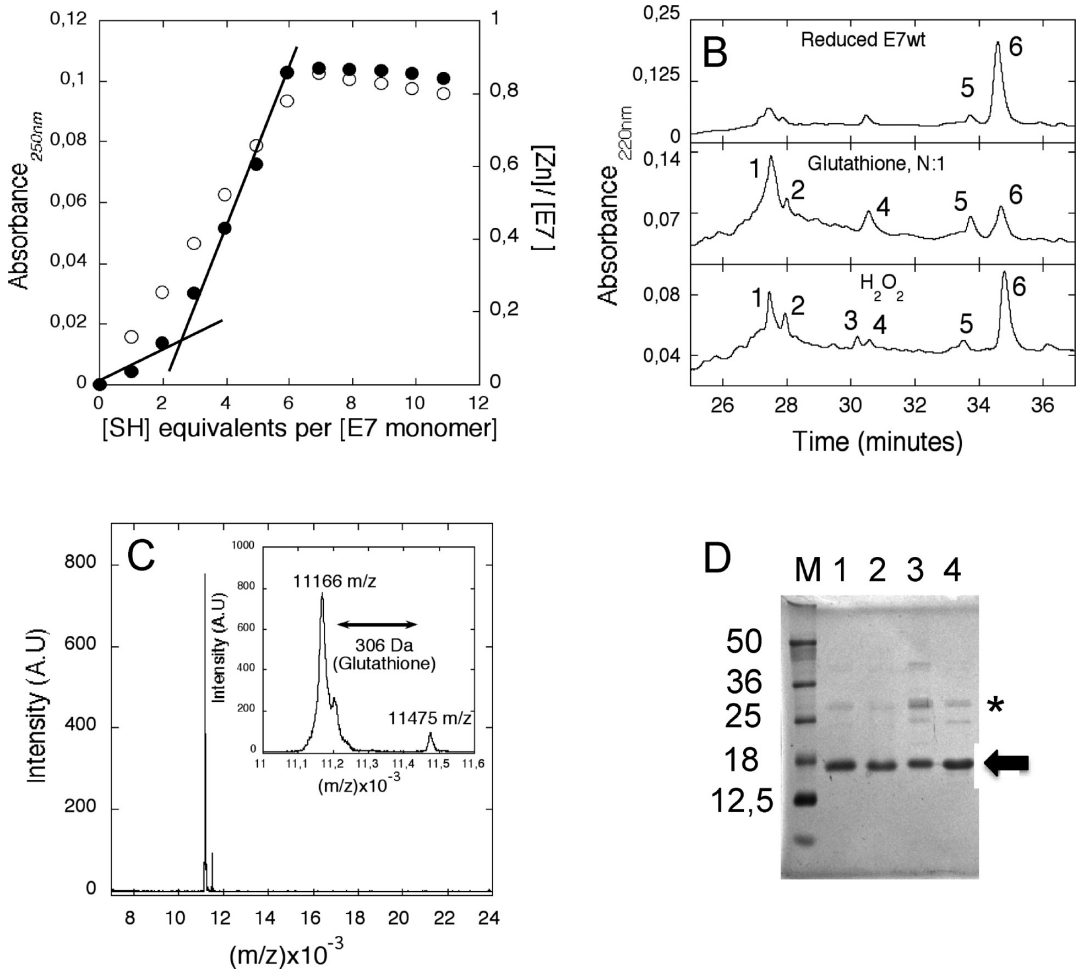

Figure 2. Basal redox state and oxidation behavior of the E7wt protein. (A) Cysteine sulfhydryl titration and Zn release of purified E7wt protein. Cysteine residues were titrated by the addition of PMPS, and the formation of thiol-mercuric bonds was followed by recording the absorbance at 250 nm (open circles). In an independent experiment, Zn release from E7wt was induced by the addition of PMPS, and released Zn was detected by the colorimetric reagent PAR to obtain the Zn to protein molar ratio (full circles). The *x*-axis represents the ratio of PMPS [SH] molar equivalents per E7 monomer molar equivalents. (B) Effect of different oxidation agents on the E7wt protein analyzed by RP-HPLC. Upper panel: RP-HPLC chromatogram of the E7wt protein incubated for 18 h with glutathione at a [GSH]:[GSSG] ratio of *N*:1000 (reducing conditions). Middle panel: RP-HPLC chromatogram of the E7wt protein incubated for 18 h with glutathione at a ratio of *N*:1 (oxidative conditions). Bottom panel: RP-HPLC chromatogram of the E7wt protein incubated for 18 h with 0.15 mM of H_2O_2. E7wt concentration was 15 μM. Peaks are identified with a number according to their order of elution in the chromatogram, with peak 6 corresponding to the fully reduced protein. (C) MALDI-TOF spectrum of the E7wt protein incubated with glutathione at ratio of *N*:1. Inset, detail of the major peak and mixed disulfide peak areas. (D) SDS-PAGE of the E7wt protein. Lane M: molecular weight markers expressed in KDa. Lane 1: E7wt oxidized with glutathione at a ratio of *N*:1. Lane 2: reduced stock E7wt sample. Lane 3: E7wt oxidized plus the addition of IAA in the cracking buffer. Lane 4: reduced stock E7wt sample plus the addition of IAA in the cracking buffer. Arrow, major monomeric E7wt species found; ∗, minor dimeric E7wt species.

buffer solution. Samples were allowed to equilibrate for at least 2 min in order to ensure that measurements were performed at steady state.

Data Analysis and Fitting. In order to obtain the K_D values for each interaction, the anisotropy values as a function of RbAB concentration were fit to the quadratic equation

$$Y = Y_F + \frac{(Y_B - Y_F)}{P_o} \cdot \frac{(x + P_o + K_D) + \sqrt{(x + P_o + K_D)^2 - (4P_o x)}}{2}$$

where Y_F and Y_B are the signal of free and bound peptide, K_D is the dissociation constant and P_o is the total peptide concentration. Data fitting was performed with ProFit (Quantumsoft, Zurich). To test whether reduction of the oxidized E7N yielded a species competent for RbAB binding, the reaction mixture obtained at the end point of the titration (100 nM oxidized FITC-E7N and 1 μM RbAB) was reduced by the addition of 5 mM DTT and the fluorescence anisotropy was followed over time.

Circular Dichroism (CD) and Fluorescence Spectroscopy. CD measurements were carried out on a Jasco J-810 spectropolarimeter (Jasco, Easton, MD) employing a scan speed of 20 nm/min, a band-pass of 1 nm, and average response time of 4 s. All spectra were an average of at least 5 scans. Temperature was maintained constant using a Peltier temperature-controlled sample compartment. Spectra of reduced and oxidized E7 at a concentration of 10 μM were taken on 0.1 cm path length cells in 10 mM potassium phosphate buffer, pH 7.5. Fluorescence emission scans were taken on a FP-6500 spectrofluorometer (Jasco, Easton, MD).

dx.doi.org/10.1021/bi401562e | *Biochemistry* 2014, 53, 1680−1696

E7 Sequence Analysis, Modeling, and Cysteine Exposure Calculations. *Alignments.* Alignments for high risk HPV E7 protein sequences were performed using the MUSCLE algorithm[46] and manually edited using the SeaView software.

Modeling of the HPV16 E7 Monomer. Three-dimensional models for the HPV16 E7 monomer were obtained by using Modeler v9.7 (http://salilab.org/modeller/)[47,48] using the HPV45 E7 monomer structure (PDB id: 2EWL) as a template. The model for the HPV16 E7 dimer was obtained by structural alignment of HPV16E7 monomers to the HPV45 dimer structure (PDB id: 2F8B) using the PyMol software (http://www.pymol.org/).

Fractional Cysteine Exposure. Raw solvent accessibility values, measured in Å^2, for each residue in the HPV45 E7 structure (PDB id: 28FB) and in the HPV16 E7 model were calculated by using the DSSP algorithm[49] implemented by the Centre for Molecular and Biomolecular Informatics (http://www.cmbi.ru.nl/dssp.html). Raw accessibility values obtained for each residue were normalized taking into account the maximal accessibility for each aminoacid, also measured in Å^2.[49]

RESULTS

Redox Behavior of Cysteine Residues in the E7 HPV16 Protein. The HPV16 E7 protein was recombinantly expressed to obtain a pure and conformationally homogeneous sample that contains a tightly bound Zn atom per E7 monomer.[20] This protein sample is routinely stored at pH 7.0 in mild reducing conditions (1 mM DTT) for several months without modifications in its oligomeric or redox state. However, the oxidation state of each of the seven cysteine residues in HPV16 E7 had not been previously assessed. In order to address this issue, a sulfhydryl titration was performed on a HPV16 E7 stock sample lacking reductant using the organomercuric reagent PMPS, which shows a high reactivity and selectivity for thiols.[43] The full-length wild type E7 protein stock (E7wt onward) was stepwise titrated with quantified aliquots of PMPS and the reaction followed by absorbance at 250 nm (Figure 2A). A linear increase in absorbance was observed with the titration of seven cysteine equivalents per E7 monomer, indicating that all cysteine residues in the sample were reduced. Independent measurements of PMPS-induced Zn-release were performed by preincubating E7wt samples with the PAR reagent and following PAR-Zn complex formation following PMPS addition by absorbance at 500 nm. The titration of ca. seven cysteines by PMPS was also required to produce the complete release of Zn from the E7wt protein (Figure 2A).

However, the Zn release curve showed two different slopes, with the titration of the first three sulfhydryl equivalents by PMPS not leading to stoichometric metal release. These results could reflect the expected differences in reactivity of free cysteines (CYS 24, 59, and 68), which account for the first slope, and Zn-coordinating cysteines (CYS 58, 61, 91, and 93) that account for the second slope. It should be noted that due to the hydrophobic nature of PMPS, no differences in cysteine reactivity based on their accessibility are expected.

Quantitative determination of the reactive cysteines with DTNB yielded 6.3 ± 0.3 mol of cysteine per mole of protein (not shown) in excellent agreement with the PMPS titration experiments. MALDI-TOF analysis of the stock E7wt protein yielded a main molecular ion mass $[M + H]^+$ of 11170.8 m/z, which can be assigned, considering the experimental error (0.1%) to the monomeric E7 protein with an expected molecular weight of 11167.5 Da (Supplementary Figure S1) for the fully reduced protein. Moreover, the presence of oxidized dimeric or oligomeric species was not observed. Altogether, these results indicated that all seven cysteine residues in the stock E7wt protein were in their reduced state. No evidence of protein oxidation was observed during protein storage, despite the absence of reductant in the storage buffer.

Next, we assessed the redox behavior of E7wt under oxidative stress conditions using two biologically relevant oxidants: glutathione and hydrogen peroxide. Glutathione is the main redox buffer in the cell,[50] and varying the reduced over oxidized glutathione (GSSG) ratio allows us to control the redox potential,[41] while the H_2O_2 molecule is a common although rather nonspecific oxidant stimulus in living cells.[51] The E7wt stock solution incubated in reducing and oxidizing conditions was resolved by RP-HPLC (see Materials and Methods). The E7wt protein stock incubated overnight in a reducing condition with a total glutathione concentration of 5 mM at a ratio of N:[GSH]/[GSSG] of 1000 at 8 °C eluted as a main peak (peak 6) at ∼34.6 min (Figure 2B, upper panel) with minor low intensity peaks, identical to the profile observed for the reduced E7wt stock sample without glutathione incubation (not shown), confirming its reduced condition. The incubation of E7wt in mild oxidative conditions (N:1) at 8 °C led to a decrease in the intensity of peak 6 and to the appearance of four additional peaks in the RP-HPLC chromatogram (Figure 2B, middle panel). The most intense peak (peak 1) showed a retention time of ∼27 min. The treatment of E7wt with 0.15 mM H_2O_2 at 37 °C for 30 min led to protein oxidation and to the appearance of 5 additional peaks (Figure 2B, bottom panel). The most intense peak observed in the peroxide-oxidized E7 chromatogram (peak 1) also showed a retention time of ∼27 min, identical within experimental error to that observed using glutathione.

Although both glutathione and H_2O_2 are considered as generic oxidants, the mechanism and nature of the chemical modification produced in proteins can differ. Glutathione is a rather specific oxidant and can form mixed disulfides with protein cysteines (S-glutathionylation) or promote the formation of intra- or intermolecular disulfide bridges. On the other hand, H_2O_2 is less specific and can oxidize cysteine to sulfenic, sulfinic, and sulfonic acid, as well as other side chain groups including methionine, tyrosine, histidine, and tryptophan.[52] Despite the mechanistic and chemical differences between both oxidants, the chromatographic profiles obtained after oxidation were very similar (i.e., the same number and retention time for each peak) (Figure 2B), suggesting that the oxidized products were comparable. The higher specificity of glutathione for studying cysteine oxidation led us to continue experiments using this reagent.

We further analyzed oxidation products using mass spectroscopy and SDS-PAGE techniques.

The glutathione-oxidized (N:1) E7wt sample containing at least 70% of peak 1 species (Figure 2B) presented a major ion of 11166 m/z (Figure 2C). At this point we were unable to discriminate whether this molecular mass peak corresponded to fully reduced E7 or to an E7 monomer containing one or more intramolecular disulfide bridges, since the expected mass difference of 2 Da for formation of a single disulfide bridge is below the technique resolution for this molecular mass range (10 Da, 0.1%). However, the fact that no covalent dimers or oligomeric species were detected by MALDI-TOF suggested that the oxidation event triggered by glutathione could

dx.doi.org/10.1021/bi401562e | Biochemistry 2014, 53, 1680−1696

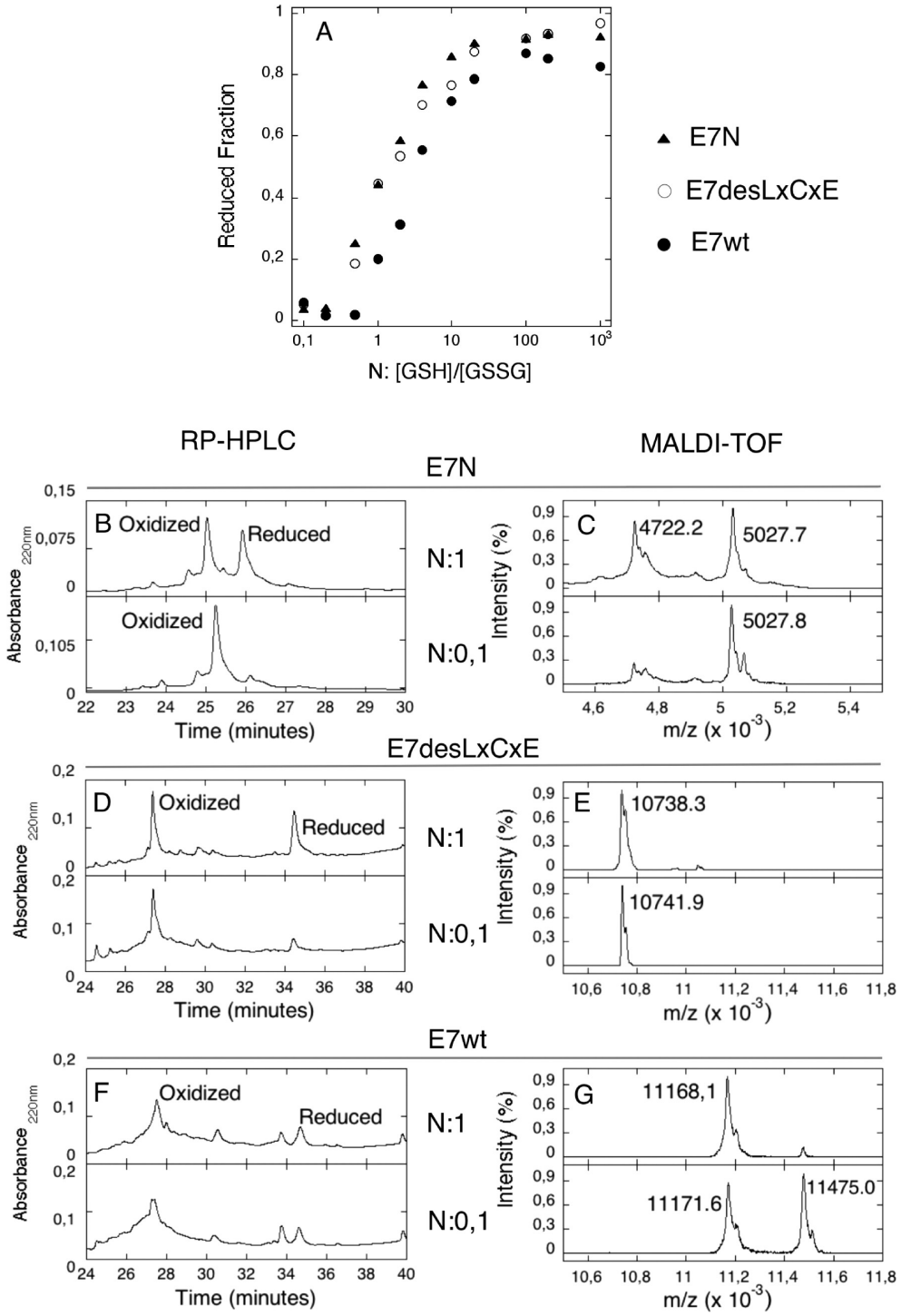

Figure 3. Assessment of redox centers in the E7 protein. (A) Redox titration of E7 variants in glutathione redox buffer. Each point corresponds to an independent sample incubated overnight at the stated [GSH]:[GSSG] *N* ratio: E7N (▲); E7desLxCxE (○); E7wt (●). (B) RP-HPLC chromatogram and (C) MALDI-TOF spectrum of E7N incubated at a ratio of *N*:1 (upper panel) or *N*:0.1 (lower panel). (D) RP-HPLC chromatogram and (E) MALDI-TOF spectrum of E7desLxCxE incubated at a ratio of *N*:1 (upper panel) or *N*:0.1 (lower panel). (F) RP-HPLC chromatogram and (G) MALDI-TOF spectrum of E7wt incubated at a ratio of *N*:1 (upper panel) or *N*:0.1 (lower panel). The chromatogram and MALDI-TOF spectrum of E7wt at a ratio of *N*:1 are the same shown in Figure 2B and are presented here for comparative purposes. Observed *m*/*z* values for major peaks are reported in each MALDI-TOF spectrum. Minor shifts in the retention time for the same species at the different *N* ratios are observed and can be expected due to experimental variability.

correspond to an intramolecular oxidation event involving cysteines or to the formation of mixed disulfides.

Although a minor peak matching the molecular weight of the protein plus one glutathione molecule (307.3 Da) was observed (11475 *m*/*z*, Figure 2C, inset), its low intensity suggested that mixed disulfides were underrepresented in the glutathione-oxidized sample at this *N* ratio. An SDS-PAGE experiment further confirmed that oxidized E7wt was mainly monomeric, as no major differences were observed when comparing oxidized

dx.doi.org/10.1021/bi401562e | *Biochemistry* 2014, 53, 1680−1696

and reduced E7wt samples or oxidized and reduced E7wt treated with IAA to quench residual reductant equivalents (Figure 2D).

Dissecting Redox Changes in the E7 Protein. A protein with seven cysteines can undergo several oxidation reactions including the formation of many potential disulfide bridges between either of its residues, making identification of the redox center experimentally complex. To address this problem, we took a fragmentation approach and first assessed the oxidative behavior of the chemically synthesized 40-residue encompassing the entire HPV16 E7N domain, which includes cysteine 24 from the LxCxE motif (Figure 1). Additionally, we obtained an HPV16 E7 mutant where amino acids LYCYE corresponding to the Rb binding site (positions 21−26 of the HPV16 sequence) were mutated to the SSAAA sequence. In this mutant, named E7desLxCxE, all remaining cysteines are located in the globular C-terminal domain (Figure 1).

E7wt, E7N, and E7desLxCxE were incubated overnight in phosphate buffer pH 7.5 at variable glutathione *N* ratios. The redox reaction was quenched by the addition of 0.1% TFA, and reduced and oxidized species were resolved by RP-HPLC and quantified by integration of peak areas. The E7wt protein showed a redox transition with an increase in the reduced fraction as *N* became higher (i.e., increase the GSH proportion) (Figure 3A). We further observed that the E7N and E7desLxCxE could be independently oxidized by increasing the GSSG concentration (Figure 3A), although the *N* range at which the oxidation reaction occurred varied for each protein. On the basis of the experimental data, we can conclude that the cysteine 24 present in the E7N can be readily oxidized, whereas on the other hand the elimination of the cysteine 24 in the E7desLxCxE protein does not preclude the oxidation of this mutant. The *N* ratio at which the E7N and E7desLxCxE oxidation occurs is roughly the same. Our interpretation is that in the full length protein two redox centers could coexist, one at the cysteine 24 (reported by the oxidation of the E7N) and the other involving one or more cysteines at the C-terminal domain (reported by the oxidation of the E7desLxCxE protein). However, whether these two potential redox centers are independently oxidized in the E7wt protein required further experimental analysis.

To gain information on the chemical nature of the redox modification occurring in the IDD N-terminal and globular C-terminal E7 domains, we further analyzed the redox curve by RP-HPLC and MALDI-TOF, with representative profiles in mild (*N*:1) and strong (*N*:0.1) oxidizing conditions shown in Figure 3B−G. E7N showed two well resolved peaks by RP-HPLC at a ratio of *N*:1, with the oxidized and reduced peaks eluting at roughly 25 and 26 min, respectively (Figure 3B, upper panel). When this sample was analyzed by MALDI-TOF, two species were identified: one with an observed molecular ion mass of $[M + H]^+$ of 4722.2 m/z corresponding to the unmodified peptide (expected $[M + H]^+$ 4720.0 m/z) and a second assigned to a mixed disulfide between the peptide and glutathione (observed $[M + H]^+$ = 5027.7 m/z, expected $[M + H]^+$ = 5025.3 m/z) (Figure 3C, upper panel). When E7N was incubated at a ratio of *N*:0.1 (10 times more GSSG over GSH), only one peak corresponding to the oxidized species was observed both in the RP-HPLC chromatogram (Figure 3B bottom panel) and the MALDI-TOF spectrum showed a single peak assigned to an E7N-glutathione mixed disulfide (observed $[M + H]^+$ = 5027.8 m/z) (Figure 3C, bottom panel). On the basis of these results, we fit the titration data to a model that considers the formation of a single mixed disulfide bridge between glutathione and cysteine 24:

$$P(SH) + GSSG \leftrightarrow PSSG + GSH$$

Using this model, we obtained a K_{mix} of 1.04 ± 0.09 for cysteine 24 (Supplementary Figure S2). The fact that the value obtained is very close to the K_{mix} values reported for the formation of mixed disulfides in free cysteine and glutathione ($K_{mix} \approx 1$),[41] reflects the solvent accessible structural environment of cysteine 24, which is located within an intrinsically disordered domain.[23]

The E7desLxCxE protein incubated at ratio of *N*:1 showed two well resolved peaks at roughly ∼27 and ∼34.6 min corresponding to similar amounts of the oxidized and reduced species, respectively (Figure 3D, upper panel). However, MALDI-TOF analysis identified one major molecular ion of 10738.3 m/z and only trace amounts of mixed disulfide (Figure 3E, upper panel). The observed signal ($[M + H]^+$ = 10738.3 m/z) could correspond either to fully reduced ($[M + H]^+$ = 10738.9 m/z) or to oxidized protein containing one internal disulfide ($[M + H]^+$ = 10736.9) within experimental error, since the 2 Da mass loss produced by the formation of an internal disulfide is beyond the resolution of the technique at high (11 KDa) molecular weight. At *N*:0.1, E7desLxCxE presented one major RP-HPLC peak representing over 80% of the total sample based on quantitative analysis, with a retention time of ∼27 min (Figure 3D, bottom panel). MALDI-TOF identified a single major molecular ion of 10741.9 m/z (Figure 3E, bottom panel). The fact that no mixed disulfide was observed in the fully oxidized sample suggested that this species contained an internal disulfide bridge, although as explained above this could not be assigned using only this technique. Therefore, on the basis of these results we concluded so far that an oxidation event involving cysteine residues located in the E7 C-terminal domain takes place that does not involve the formation of a mixed disulfide.

The chromatogram and MALDI-TOF spectrum of E7wt incubated at a ratio of *N*:1 was previously described (Figure 2) and is shown here for comparative purposes (Figure 3F and G, upper panel). The chromatogram profile of E7wt incubated at a ratio of *N*:0.1 (Figure 3F, lower panel) showed no major differences with the data for *N*:1, except for the broadening of peak 1 eluting at 27 min. However, as opposed to the single species observed at *N*:1, MALDI-TOF analysis at *N*:0.1 showed two major species, one with a molecular ion of $[M + H]^+$ = 11171.6 m/z corresponding to the reduced protein or to the protein with an internal disulfide and a second molecular ion $[M + H]^+$ = 11475.0 m/z corresponding to the mixed disulfide between the E7wt protein and one glutathione molecule (Figure 3G, lower panel).

This set of data can be interpreted by proposing that E7 can suffer two distinct redox modifications. The first corresponds to the formation of an intramolecular disulfide bridge involving cysteine residues located in the globular C-terminal domain, which produces a strong retention time shift of the full-length protein by RP-HPLC (∼7.6 min, from 34.6 to 27 min). Second, we propose the formation at higher *N* ratio of a stable mixed disulfide bridge involving cysteine 24 located in E7N. This oxidation event does not produce a retention time shift in RP-HPLC, which could be explained by the highly hydrophilic nature of the N-terminal domain where the mixed disulfide occurs. However, this oxidation event may be responsible for the broadening of peak 1 at 27 min corresponding to oxidized E7wt, a conclusion supported by the fact that this broadening is not observed in oxidized E7desLxCxE, which lacks cysteine 24. The absence of cysteine 24 in E7desLxCxE prevents mixed-disulfide formation, coincident with the fact that this modification was not

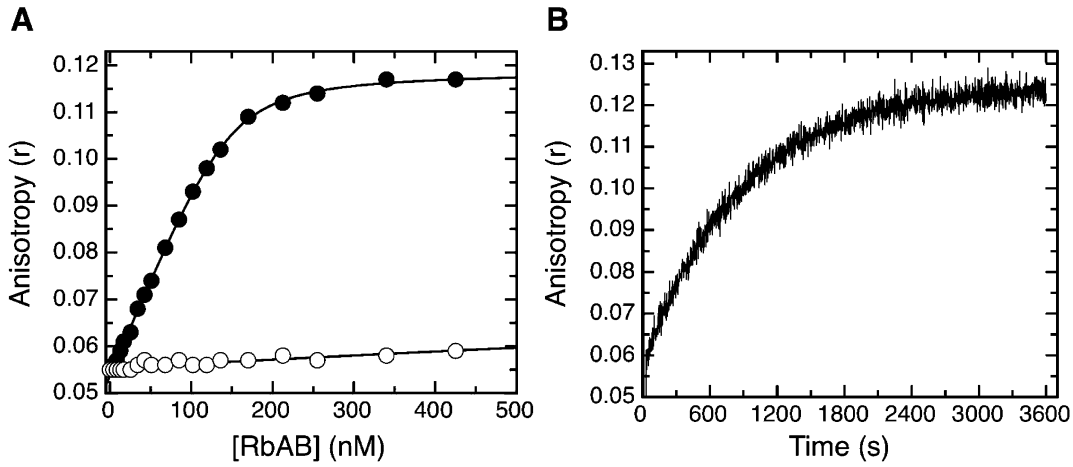

Figure 4. Binding properties of reduced and gluthtionylated E7N to the RbAB domain. (A) Binding curve for the reduced (●) and gluthatione-oxidized (○) E7N domain (E71-40) to the RbAB domain. The different peptides were FITC-labeled, and anisotropy at 520 nm was measured. E7N concentration was 100 nM. The affinities calculated by curve fiting were K_D = 8.6 ± 1.0 nM for reduced E7N and K_D > 6.8 ± 0.9 μM for oxidized E7N. (B) Recovery of RbAB binding of oxidized E7N upon reduction with DTT. For reduction, 5 mM DTT was added to the cuvette at the end point of the titration shown in panel A (time zero). After this, fluorescence anisotropy was followed over time, showing an increase from levels characteristic of no binding (r = 0.06), to levels correponding to E7N being fully reduced and bound to RbAB (r = 0.124).

observed in samples oxidized at a ratio of N:0.1 (Figure 3E, lower panel). The hydrophilic nature of the E7N domain may also explain why the mutation of residues 21−26 in the E7desLxCxE protein has no major impact on the overall reverse-phase binding behavior and retention time of the reduced and oxidized species in comparison to the E7wt protein.

Interestingly, a different behavior of E7N and the E7wt protein with respect to the formation of a mixed disulfide bridge involving cysteine 24 should be noted. While E7N is fully glutathionylated at a ratio of N:0.1 (Figure 3C, lower panel), the E7wt protein is only partially glutathionylated at the same N ratio (Figure 3G, lower panel), indicating that cysteine 24 is partially protected from oxidation when found in the context of the full length protein.

Binding of Reduced and Oxidized E7N Species to the RbAB Domain. The finding that Cys 24, central to the Rb-binding LxCxE motif, could be readily gluthationylated prompted us to investigate the binding properties of the oxidized E7N domain. For this purpose, we performed equilibrium binding experiments, where we tested binding of the reduced and oxidized FITC-labeled E7N domain. RbAB binding of reduced E7N was measured in buffer containing 2 mM DTT, and we obtained a K_D value of 8.6 ± 1.0 nM (Figure 4A) and fluorescence anisotropy values of free and bound peptide of 0.054 and 0.12 respectively, in very good agreement with previously reported values.[45] In contrast, binding of the oxidized E7N peptide to RbAB was negligible with a final anisotropy value at the end point of the titration of only 0.06, close to the value of free peptide, and a 1000-fold reduction in binding affinity to a K_D value of 6.8 ± 0.9 μM (Figure 4A). In order to test whether this drop in binding affinity depended on oxidation of Cys 24 within the LxCxE motif, we added 5 mM DTT to the reaction mixture at the end point of the titration, containing 100 nM oxidized FITC-E7N and 1 μM RbAB, concentrations that led to full binding of the reduced peptide (Figure 4A). As it can be observed, DTT addition led to a slow increase in the anisotropy from a value of 0.06 to a final value of 0.124, characteristic of fully bound peptide (Figure 4B), indicating that gluthationylation of Cys 24 was a reversible process, and that Rb-binding affinity was restored upon Cys 24 reduction. As binding of E7N to RbAB has been shown to be a very fast process occurring in the millisecond time scale (k_{on} = 2.5 × 10^7 M^{-1} s^{-1}),[53] the slow increase in anisotropy value reflects a slow kinetics of reduction of the mixed disulfide upon DTT addition.

Mapping Cysteine Connectivity in Oxidized E7. Since MALDI-TOF analysis of full length E7wt did not allow characterization of intramolecular disulfide bridges, further characterization of oxidized species was performed using a fragmentation approach. As opposed to the direct identification of the chemical species of the redox change that occurs in the single cysteine contained within E7N, determination of the cysteine connectivity in the C-terminal domain (containing six cysteines) was a complex task that required thiol alkylation followed by protein proteolysis and subsequent MALDI-TOF analysis.[54] This strategy allows discrimination of cysteines that are in their thiol-reduced state, which are readily alkylated with iodoacetamide (IAA), from cysteines that are forming a disulfide bridge and are therefore not reactive. Cysteines involved in disulfide bridge formation can be further identified through the direct observation of disulfide-linked peptides. We evaluated cysteine connectivity using the oxidized E7desLxCxE protein, which was highly enriched in the peak 1 species (>80% peak area, Figure 3D) observed in both gluthatione and peroxide oxidized samples (Figure 2B). To this end, we prepared an oxidized E7desLxCxE sample highly enriched in peak 1 species as described in materials and method.

Although ∼80% of E7desLxCxE protein is oxidized and present in peak 1 at N:0.1, a residual amount of reduced protein can account for low intensity fully reduced peptides that could be observed in the MALDI-TOF experiment. E7 HPV16 is an acidic protein with only four R or K residues, which constitute targets for trypsin cleavage and are distributed over the E7 sequence yielding five digestion peptides (T1−T5) that allow characterization of most of the cysteine residues within E7 (Figure 5A). Three different representative samples were analyzed by MALDI-TOF: (i) oxidized E7desLxCxE protein treated with IAA and cleaved with trypsin; (ii) oxidized E7desLxCxE protein that was treated with IAA, reduced with DTT, and cleaved with trypsin; and (iii) a control stock sample of reduced E7desLxCxE protein that was treated with IAA and cleaved with trypsin. The

dx.doi.org/10.1021/bi401562e | Biochemistry 2014, 53, 1680−1696

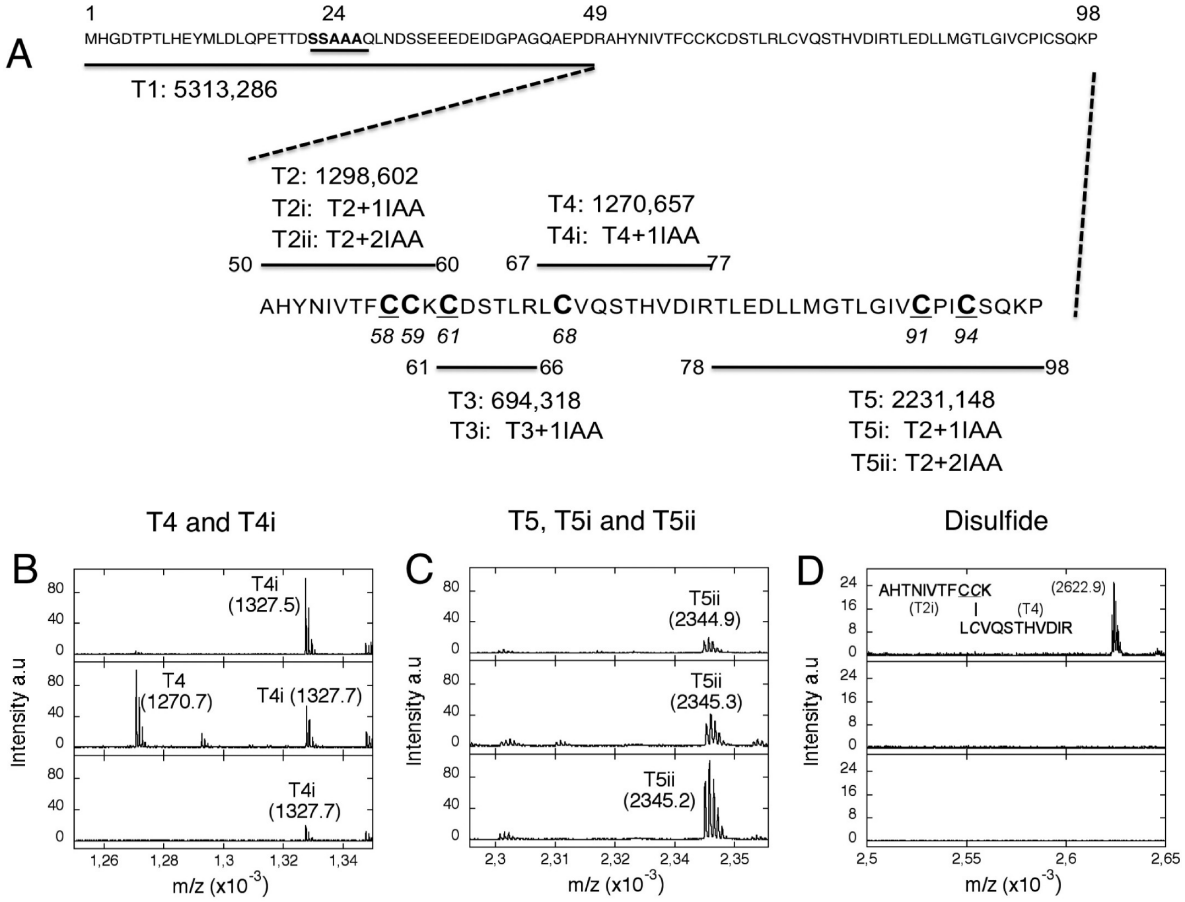

Figure 5. Identification of a disulfide bridge in oxidized E7desLxCxE. (A) Schematic representation of peptide fragments digestion expected after trypsin proteolysis of E7desLxCxE. Fragments are named by the letter T followed by a number that indicates the order of appearance in the primary sequence. All fragments contain cysteines that can be derivatized with IAA; the number of alkylated cysteines present in each fragment is indicated by the lower case letter i. Cysteines 58, 61, 91, and 94 involved in Zn binding are underlined and in bold, while noncanonical cysteines 59 and 68 are in bold. The region mutated in E7desLxCxE encompassing the Rb binding site in E7N (see fragment T1) is underlined and in bold. (B) MALDI-TOF spectra showing the T4 family ion. (C) MALDI-TOF spectra showing the T5 family ion. (D) MALDI-TOF spectra showing the disulfide-bound fragment of 2623.2 *m*/*z*. A schematic representation of the T2i and T4 fragments linked by a disulfide bridge is presented in the upper panel. Since the T2 fragment contains two cysteine residues (Cys 58 and 59) that are able to form a disulfide bridge, a peptide mass shift of 57 Da is observed due to the addition of one molecule of IAA. (B–D) Upper panel: oxidized E7desLxCxE sample with IAA. Middle panel: oxidized E7desLxCxE reduced with DTT after IAA addition. Lower panel: reduced E7desLxCxE sample with IAA.

Table 1. MALDI-TOF Identification of the IAA-Alkylated Fragments Obtained by the Treatment of E7desLxCxE Samples with Trypsin

fragment	expected monoisotopic $(M + H)^+$	cysteine no.	IAA	oxidized E7desLxCxE[a]	oxidized E7desLxCxE + DTT[a]	reduced E7desLxCxE[a]
T2	1298.6	58–59	0	nd	nd	nd
T2i	1355.6	58–59	1	nd	nd	nd
T2ii	1412.6	58–59	2	li	nd	li
T3	694.3	61	0	nd	nd	nd
T3i	751.3	61	1	751.2	751.3	751.3
T4	1270.7	68	0	li	1270.7	nd
T4i	1327.7	68	1	1327.5	1327.7	1327.7
T5	2231.1	91–94	0	nd	li	nd
T5i	2288.3	91–94	1	nd	li	nd
T5ii	2345.2	91–94	2	2344.9	2345,3	2345.2
T4-s-s-T2i	2623.3	58–59 and 68	1	2622.9	nd	nd

[a]nd, not detected; li, low intensity, less than 10% of the most intense fragment.

results from one representative experiment are shown in Table 1. For each peptide, a series corresponding to the degree of alkylation with IAA is reported (Figure 5A and Table 1). We classified the observed ions in three main groups according to their intensity: not detected ions (nd), ions detected at low (less than 10%) intensity (li), and ions detected at high intensity for which the observed *m*/*z* is shown in Table 1. Peptide T1 with an estimated molecular weight of 5313.3 Da (Figure 5A)

dx.doi.org/10.1021/bi401562e | *Biochemistry* 2014, 53, 1680–1696

corresponding to the first 49 amino acids of E7desLxCxE does not contain cysteine and was excluded from the analysis.

The T2, T2i, and T2ii peptide family containing cysteines 58 and 59 modified with none, one, or two IAA moieties constitutes a peptide family that was poorly detected or not detected in all samples including the control reduced E7desLxCxE protein. Among the peptides that contain cysteine 61 (T3 and T3i) only the alkylated peptide T3i was detected with high intensity in all samples, indicating that cysteine 61 is reduced in the oxidized E7desLxCxE protein. The peptide family containing cysteine 68 (T4 and T4i) showed a clear differential pattern in the oxidized and the reductant-treated oxidized sample. In oxidized E7desLxCxE, only the alkylated T4i peptide was detected, suggesting the presence of a residual population of cysteine in a reduced state. In the oxidized E7desLxCxE sample treated with DTT, both peptides were clearly detected (Table 1 and Figure 5B). In this last sample, the intensity of the T4 ion was higher than the T4i ion, suggesting that two protein populations coexist in the oxidized sample, one with cysteine 68 in its reduced form (yielding the T4i peptide) and the other with cysteine 68 forming a disulfide bridge and therefore not reactive toward IAA (yielding the T4 peptide). In the reduced sample only the alkylated T4i peptide was detected. The peptide family containing cysteines 91 and 94 (T5, T5I, and T5ii) did not show a differential pattern between the three samples, and T5ii was the only species detected (Table 1 and Figure 5C), indicating that cysteines 91 and 94 are not forming a disulfide bridge in oxidized E7desLxCxE.

A strong positive evidence supporting the existence of a disulfide bridge was the systematic detection of a peptide of $[M + H]^+ = 2623.3$ m/z in the oxidized E7desLxCxE sample that was assigned to a fragment containing peptides T4 (cysteine 68) and T2i (cysteines 58 and 59) linked by a disulfide bridge (Table 1 and Figure 5D, upper panel). This fragment was not observed either in the oxidized E7desLxCxE sample treated with DTT or in the reduced E7desLxCxE stock sample (Figure 5D, middle and lower panel). In order to confirm this result, cysteine connectivity was further analyzed using *N*-ethylmaleimide (NEM) as a thiol-modifying agent. The second order rate constant for the reaction of an average thiol with IAA (pH ≈ 8) was 4.6 M^{-1} s^{-1}, while NEM reacted 200-fold faster with a constant of 10000 M^{-1} s^{-1}.[41] This large difference in reactivity toward thiols can be useful to prevent rapid disulfide reshuffling that can occur during sample handling.

The results for the NEM experiments are shown in Supplementary Figure S3 and tabulated in Supplementary Table 1. The results obtained with NEM fully support those shown for IAA, with the same observed patterns of ions compared to the IAA experiment. The TN2 ion family was poorly detected as isolated fragments. Only TN3i was detected, indicating that cysteine 61 was in its reduced form in the three samples. The TN4 and TN4i peptides showed a clear differential pattern in the oxidized and the oxidized plus DTT sample, with the intensity of the TN4 ion being higher than the T4i ion in the oxidized E7desLxCxE sample treated with DTT, indicating a partial oxidation of cysteine 68 (Supplementary Figure S3). Cysteines 91 and 93 were found in their reduced state and reacted with NEM, yielding mainly the TN5ii (Supplementary Figure S3). Finally, an ion of $[M + H]^+ = 2691.2$ m/z was observed in the oxidized sample only and could be assigned to a fragment containing the TN4 and TN2i peptides linked by a disulfide bridge (Supplementary Figure S3). Note that the difference in the molecular weight of the disulfide-linked fragment obtained in the NEM experiment versus the IAA experiment is due to the differences in the molecular weight of both reagents (IAA = 57 Da vs NEM = 125 Da). Taken together, these data indicate that peak 1 corresponds to an oxidized species containing an internal disulfide bridge between cysteine 68 and either cysteine 58 or 59. Since both cysteines 58 and 59 are contained within the same tryptic peptide (T2 peptide family), this approach did not allow discriminating which cysteine was involved in the disulfide bridge. Remarkably, three of the four cysteine residues involved in Zn coordination (C61, C91, and C94) were protected from oxidation, suggesting that C58 may also be protected from oxidation and encounter a structural role in oxidized E7.

Effect of C59A Mutation on E7 Redox Behavior. In order to test whether cysteine 58 or 59 was the residue involved in the disulfide bridge with cysteine 68, we obtained the E7C59A mutant, which does not alter Zn-binding cysteines (Figure 1). The C59A mutation had no effect on Zn coordination or on protein stability as judged by PMPS-PAR and circular dichroism (CD) measurements (not shown). The formation of the disulfide-oxidized species in the E7C59A was evaluated by the appearance of peak 1 by RP-HPLC following incubation with different glutathione *N* ratios.

A first inspection of the RP-HPLC profiles in highly reducing conditions (i.e., $N \geq 200$) showed important differences between E7C59A and E7wt, with a marked increase in the content of oxidized species in the E7C59A, detected as increments in several peaks, including peak 2 and peak 4 areas (Figure 6A, upper and middle panel). The chromatogram of oxidized E7C59A at glutathione ratios of *N*:1 and *N*:0.1 was devoid of peak 1 observed in E7wt, indicating that formation of the oxidized species corresponding to peak 1 requires the presence of cysteine 59 (Figure 6B and C, upper and middle panel). This result allowed us to assign a C59−C68 connectivity for the disulfide bridge identified in oxidized E7.

The high level of oxidation observed in reducing conditions upon mutation of C59 suggested that this residue had a protective effect on the overall redox state of E7 cysteines. To further analyze this possibility, we tested oxidation in the E7C59A-desLxCxE mutant, where cysteines 59 and 24 have been replaced by alanine. Remarkably, this mutant presented a chromatogram similar to that observed for E7wt (Figure 6A, upper and lower panels). This result suggests that the presence of cysteine 59 prevents oxidation events mediated by cysteine 24. As expected by the absence of C59 in this mutant protein, no evidence for the appearance of peak 1 representing the disulfide linked species was observed upon incubation in oxidizing conditions (Figure 6B and C, upper and lower panels). Moreover, the fact that this mutant that retains C68 showed very low overall levels of oxidized species, with the exception of the nonidentified oxidized species peak X (Figure 6B and C, lower panel), was an indication that C68 had low intrinsic reactivity to oxidation. Taken together, these results confirmed that the disulfide bridge in oxidized E7 involves residues C59 and C68 and also indicated that the presence of cysteine 59 in the wild type protein prevents the formation of oxidized E7 species in reducing environments.

C59−C68 Disulfide Yields a Conformational Rearrangement in E7. Our experimental results indicated that the disulfide bridge in oxidized E7 forms between cysteines 59 and 68 and does not involve the Zn-coordinating cysteines (positions 58, 61, 91, and 94), implying that the oxidized protein is potentially able to bind the metal atom. We assessed the binding

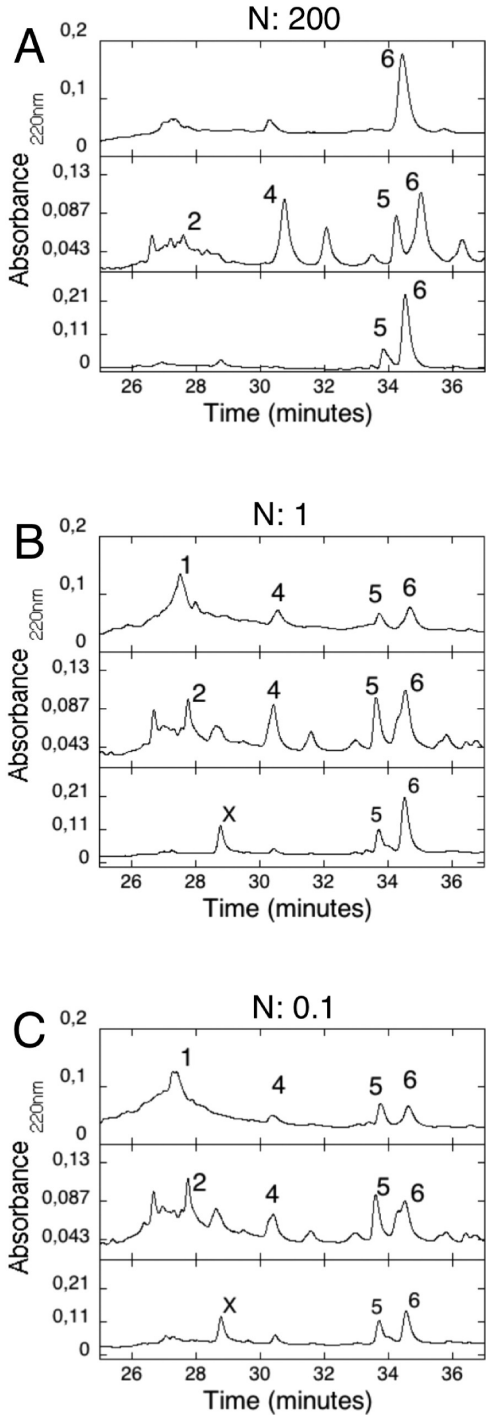

Figure 6. Effect of mutation of C59 and C59/C24 on E7 redox behavior. (A) RP-HPLC chromatogram of E7wt (upper panel), E7C59A (middle panel), and E7C59A-desLxCxE (lower panel) samples incubated with glutathione at a ratio of *N*:200 (highly reducing conditions). (B) RP-HPLC chromatogram of E7wt (upper panel), E7C59A (middle panel), and E7C59A-desLxCxE (lower panel) samples incubated with glutathione at a ratio of *N*:1. (C) RP-HPLC chromatogram of E7wt (upper panel), E7C59A (middle panel), and E7C59A-desLxCxE (lower panel) samples incubated with glutathione at a ratio of *N*:0.1 (highly oxidizing conditions). Peak numbering is as in Figure 2, with peak 6 corresponding to the fully reduced protein. Peak "X" appears only in E7C59A-desLxCxE oxidized samples.

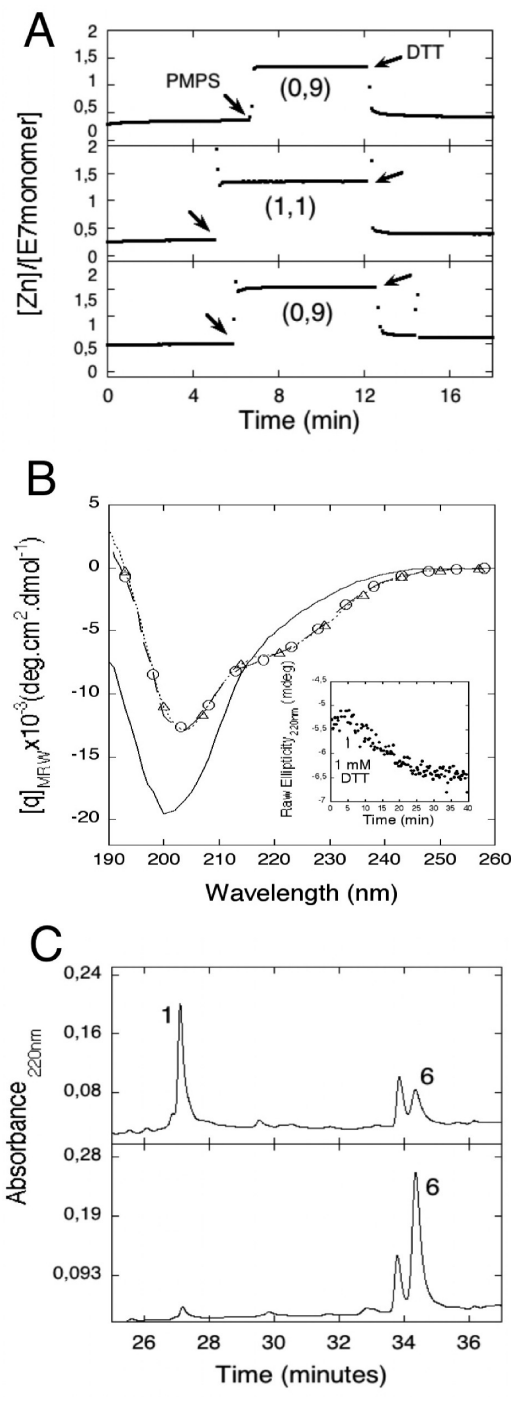

Figure 7. Metal binding and conformation of oxidized E7desLxCxE. (A) Quantitative evaluation of strongly bound Zn in oxidized E7desLxCxE (upper panel), reduced E7desLxCxE (middle panel), and reduced E7wt (lower panel). The addition of 100 μM PMPS is indicated by an arrow. Released Zn was quantified by a colorimetric reaction with PAR (see Materials and Methods). Cysteines were unblocked by the addition of 250 μM DTT, indicated by a second arrow. (B) Far-UV CD spectra of reduced E7desLxCxE (dotted line with triangles), oxidized E7desLxCxE (full line), and oxidized E7desLxCxE that had been reduced by incubating the protein for 1 h at 37 °C with 1 mM DTT (full line with circles). Inset: kinetics of reduction of oxidized E7desLxCxE followed by molar ellipticity at 220 nm, initiated by adding 1 mM of DTT at 37 °C (indicated by an arrow). (C) RP-HPLC chromatogram of oxidized E7desLxCxE before (upper panel) and after reduction with DTT (lower panel).

properties of oxidized E7desLxCxE (Figure 7A, upper panel), reduced E7desLxCxE (Figure 7A, middle panel), and reduced

dx.doi.org/10.1021/bi401562e | *Biochemistry* 2014, 53, 1680−1696

E7wt protein (Figure 7A, lower panel) using the colorimetric detection of PAR-Zn complexes.[43] Surprisingly, all three samples showed a ∼1:1 Zn:protein stoichiometry, indicating that oxidized E7desLxCxE was able to bind Zn despite the formation of a disulfide bridge between cysteines 59 and 68. We assessed the relative affinity for the Zn-protein interaction by comparing the ability of PAR to compete for the protein-bound metal. The PAR-Zn complex has a reported equilibrium constant K_d of $\sim 10^{-12}$ M,[43] and the estimated dissociation constant for the E7wt-Zn complex was lower, since 100 μM concentration of PAR present in the sample was unable to displace high affinity protein-bound Zn (Figure 7A). The addition of PMPS produced the release of Zn, which in turn formed a colored complex with PAR producing an abrupt increase of the absorbance at 500 nm (Figure 6A). The subsequent addition of DTT released PMPS-blocked cysteines, leading to Zn reuptake by the protein and to a decrease in the absorbance at 500 nm.[43] Oxidized E7desLxCxE showed a behavior similar to that observed for reduced E7desLxCxE and E7wt, suggesting that oxidized E7desLxCxE maintains its high affinity Zn-binding site and that the oxidized protein is able to reuptake the metal ion once its cysteines have been released from PMPS (Figure 7A). The protein samples contain a basal, substoichiometric amount of spurious metal detected by the level of the basal absorbance at 500 nm that corresponds to soft-bound metal, not necessarily Zn, which is readily complexed by PAR without the addition of PMPS.

According to the published structures of E7 from the HPV1A and HPV45 types,[21,22] cysteines 59 and 68 in HPV16 E7 would be located too distant from each other (18.6 Å) to be able to form a disulfide bridge without the protein suffering a considerable rearrangement in its secondary and tertiary structure (Figure 1C). To assess this point, we performed far-UV CD measurements of reduced and oxidized E7desLxCxE (Figure 7B). As a control, we compared the CD spectrum of reduced E7desLxCxE to that of reduced E7wt, which has been thoroughly characterized,[20] observing no significant differences among them (not shown). The CD spectrum of oxidized E7desLxCxE differed clearly from that of reduced E7desLxCxE (Figure 6B), presenting a decrease in the absolute value of the negative shoulder at 220 nm, assigned to an α-helical structure present in the native E7 structure (Figure 1), as well as an increase in the absolute value of the negative band at 200 nm that has been assigned to intrinsically disordered elements, likely at the E7N IDD.[20,23] Together, these results indicated that oxidized E7desLxCxE presented a loss of canonical secondary structure elements. Despite the changes observed in the protein secondary structure, oxidized E7 preserved its ability to bind Zn and reuptake it with high affinity (Figure 7A). Finally, the addition of 1 mM DTT led to a slow reversal of these structural changes (Figure 7B, inset), yielding a final CD spectrum that could be superimposed to that of the reduced protein (Figure 7B). The reversibility of the oxidation process was also verified by RP-HPLC, where addition of 5 mM DTT to an oxidized E7desLxCxE sample led to full recovery of the reduced peak 6 (Figure 7C).

DISCUSSION

E7 is a small oncoprotein that plays a crucial role in the HPV virus life cycle and in cervical cancer development in humans.[9] Considerable work has been conducted to understand its functional and structural properties; however, despite the fact that HPV16 E7 shows high cysteine content and that 12 out of the 13 high risk HPV E7 proteins contain at least two noncanonical cysteines, its redox behavior has not been investigated to date. In the present work we show the effect of oxidative conditions on E7, we describe two distinct redox centers in the HPV16 E7 oncoprotein involving cysteine 24 and the cysteine 59/68 pair, respectively, and we demonstrate the protective effect of noncanonical cysteine 59 on the overall E7 redox state.

Strictly conserved cysteines involved in Zn binding have been widely studied, revealing a marked decrease in protein stability upon mutation,[55,56] and cysteine 24 within the LxCxE motif was pointed out as an important residue for Rb binding.[57] The fact that noncanonical cysteines 59 and 68 in HPV16 E7 do not show strict conservation across papillomavirus E7 proteins may be the reason why this cysteine pair has not been previously identified as a potential site of redox regulation of E7 proteins.

Our study shows that despite its high cysteine content all seven cysteine residues within HPV16 E7 are in their reduced state under conditions that resemble the basal reducing environment of the cell cytoplasm.[50] However, E7 undergoes a controlled oxidation process upon the addition of biologically compatible oxidants such as hydrogen peroxide (H_2O_2) and glutathione (GSSG) (Figure 2). One redox center in E7 involves the solvent-exposed cysteine 24 located within the LXCXE Rb binding motif in the intrinsically disordered N-terminal domain of E7. This cysteine is readily glutathionylated in the context of the isolated E7N domain and has a K_{mix} value close to 1, similar to that observed for free alkyl thiols.[41] The fact that this residue is within a disordered domain and exposed to the solvent indicates that it could be easily oxidized (i.e., undergo redox regulation) under stress conditions. Moreover, we demonstrate that Cys 24 gluthationylation abolishes Rb-binding, a process that is fully reversible by the addition of DTT and leads to full recovery of Rb-binding (Figure 4). A second redox center is located in the E7 C-terminal domain, where we show the formation of an internal disulfide bridge between cysteines 59 and 68 through peptide mapping (Figure 5). However, our results show that in the context of the full-length protein cysteine 24 is protected from oxidation and less prone to glutathionylation than in the context of the isolated E7N peptide (Figure 3), indicating that the C-terminal cysteine-rich domain can prevent the glutathione-induced oxidation of cysteine 24. The protective effect of the E7C domain over the E7N domain strongly suggests an unexpected long-range interdomain interaction.

The fact that two very different oxidative agents lead to the same oxidized E7 end-product (peak 1) recalls canalization, an evolutionary process whereby a population produces similar phenotypes regardless of environmental variability,[58] and suggests the presence of a common and evolved oxidation mechanism. Moreover, oxidation of solvent-accessible cysteine 24 is diminished in the context of the E7wt protein (Figure 3), and removal of cysteine 59 leads to loss of peak 1 (C59−C58 disulfide bridge) and to an increase in basal-state oxidation in conditions ($N > 200$) where the wild type protein remains fully reduced, suggesting that the evolutionary conservation of noncanonical cysteines in the E7 sequence is functionally driven. Considering the fact that the E7 oncoprotein performs its functions in an oxidative environment,[16,17,19] a likely hypothesis is that noncanonical cysteines protect the E7 protein against oxidative damage and consequent loss of function as suggested by our experimental results (Figure 4). Alternatively, C24 oxidation could serve as a sensor for redox regulation of Rb binding, modulating the interaction affinity.

Analysis of surface accessibility of the positions corresponding to residues C59 and C68 in HPV16 E7 reveals that while cysteine 59 is highly exposed in both the dimeric and monomeric E7 structures (Figure 8 and Table 2), the position corresponding to

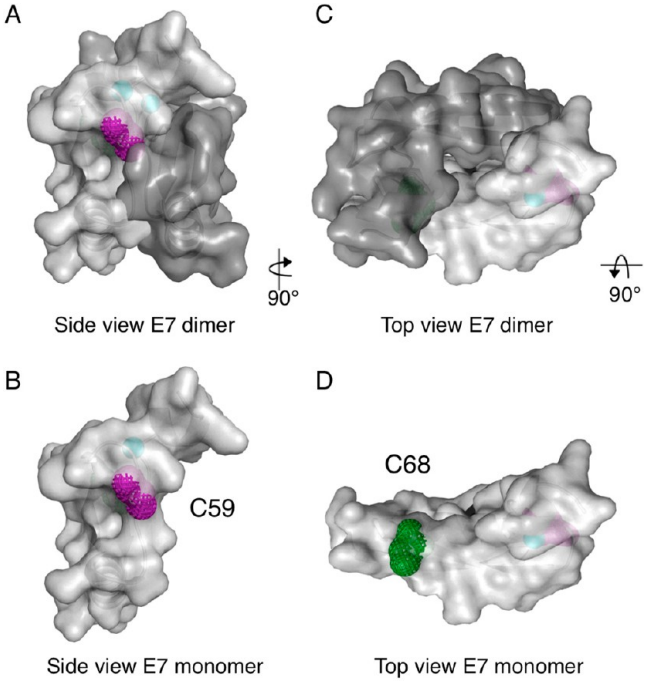

Figure 8. Changes in exposure of noncanonical cysteines in E7 upon dimer dissociation. (A, B) Side view of HPV16 E7 dimer modeled showing the changes in exposure of cysteine 59 (pink) upon dissociation of the E7 dimer. (C, D) Top view of the HPV16 E7 dimer showing the changes in exposure of cysteine 68 (green) upon dissociation of the E7 dimer. The HPV16 E7 dimer was modeled using Modeler and the HPV45 E7 dimer structure (PDB id: 2F8B) as a template, with both E7 monomers depicted in light and dark gray, respectively. The rotation of structures with respect to the orientation depicted in Figure 1B is indicated.

cysteine 68 (threonine in HPV45 E7) is fully buried in the dimer interface but becomes exposed upon dimer dissociation (Figure 8 and Table 2). Moreover, we have experimentally demonstrated that the E7 oxidation shows a marked dependence with the total protein concentration (Supplementary Figure S4), indicating that a dimer to monomer equilibrium shift led to an increase of the amount of the oxidized E7 species (peak 1). Altogether, this evidence suggests that the formation of the C59−C68 disulfide requires E7 dimer dissociation. The low amount of oxidized dimeric or oligomeric species observed in this study further suggests that oxidation may proceed through a monomeric E7 intermediate (Figure 2C), in line with the weak (~1 μM) reported dissociation constant for the E7 dimer.[24]

The distance between positions 59 and 68 within the E7 HPV16 monomer is about 18.6 Å (Figure 1). This implies that the formation of a disulfide bridge between C59 and C68 must necessarily be accompanied by a large-scale rearrangement of the protein secondary and tertiary structure. Such changes are reported by the pronounced difference between the far-UV CD spectra of the oxidized and reduced E7desLxCxE protein. Interestingly, the conformational transition induced upon E7 oxidation is fully reversible, as indicated by restoration of the reduced far-UV CD spectrum upon DTT addition (Figure 7B), supporting a regulatory role of this species. The fact that the

Table 2. Relative Accessibility for Cysteine-Rich Positions 24, 59, and 68 in E7

cysteine	location	HPV45 E7[a] dimer	HPV45 E7[a] monomer	HPV16 E7[a] monomer	experimental reactivity
24	canonical Rb binding			IDD	K_{mix} = 1[d]
58	canonical Zn binding	0	0	0	nr[e]
59	noncanonical	0.62[b]	0.63[b]	0.47	disulfide[e]
61	canonical Zn binding	0.37	0.43	0.5	nr[e]
68	noncanonical	0.007[c]	0.51[c]	0.72	disulfide[e]
91	canonical Zn binding	0.09	0.16	0.06	nr[e]
94	canonical Zn binding	0.01	0.05	0.08	nr[e]

[a]Relative accessibility for cysteine residues was calculated using the DSSP algorithm,[49] with exposed surface areas normalized per maximal residue area (see Materials and Methods). Cysteine residues with relative accessibility values >0.2 were considered accessible, and those with values <0.2 were considered buried. [b]The position corresponding to Cys 59 in HPV 16 E7 is also a cysteine in HPV45 E7. [c]The position corresponding to Cys 68 in HPV16 E7 is a threonine residue in HPV45 E7. [d]Reactivity was judged by comparison of the K_{mix} value to that of free cysteine (K_{mix} ~1).[41] [e]Reactivity was derived from oxidation followed by MALDI-TOF analysis (Figure 4 and Table 1)

oxidized species retains strong Zn coordination despite the strained conformation induced by the disulfide bridge formation, suggests that the Zn binding motif may act as a scaffold to help guide the structural changes leading back to the native state upon reduction of the disulfide bridge. In support of this mechanism, experimental evidence suggests that, with few exceptions,[59,60] Zn binding cysteines are less reactive to oxidation than others cysteines, as they are protected by metal coordination (Table 2).[61] Many proteins regulated by disulfide formation present cysteines that are far apart from each other in the reduced state. A paradigmatic example is the redox-responsive regulator OxyR, a transcription factor activated upon exposure to hydrogen peroxide.[62] This regulator forms an intramolecular disulfide bridge between cysteines located 17 Å apart in the reduced inactive form, which is accompanied by a dramatic structural change in the regulatory domain.[63] Similarly, formation of an internal disulfide bridge in intracellular chloride ion channel proteins (CLICs) induces a major structural rearrangement and changes in the oligomerization state, as revealed by crystallographic studies of the oxidized form.[64]

Cysteine 59 is located in Cluster 1, proximal to the Zn binding site of the same monomer and is exposed in both the dimer and monomer structures (Figures 1 and 8A,C). Remarkably, the position immediately following C59 is occupied by a basic residue in most HPV E7 proteins (Figure 1), a feature known to lower cysteine pK_a, increasing its chemical reactivity.[31,40,65] These structural features suggest that C59 is a highly reactive cysteine, thus likely to play a functional role. On the other hand, C68 belongs to Cluster 2 and is buried in the dimer structure, requiring monomerization in order to be exposed (Figure 8 B,D). Moreover, experiments with the E7C59A-desLxCxE variant indicate that C68 has low propensity to oxidation (Figure 5), suggesting that this cysteine has low reactivity. The presence of an exposed reactive cysteine surrounded by basic residues is a common mechanistic feature of proteins that are redox regulated due to conformational changes triggered by disulfide formation

dx.doi.org/10.1021/bi401562e | Biochemistry 2014, 53, 1680−1696

such as OxiR[63] as well as of proteins involved in redox catalysis such as peroxiredoxin.[66]

In redox regulated proteins such as OxyR, the C199 reactive cysteine has a positively charged environment and serves as the stimulus sensor, which is easily oxidized by H_2O_2, initiating a conformational change that allows for disulfide bond formation.[63] On the other hand, the existence of a highly reactive Cys may support an effective redox catalytic cycle, a mechanism that has been well studied in atypical mammalian 2-Cys peroxiredoxin (Prdx 5).[66,67] Whether noncanonical cysteines in E7 proteins possess a relevant function, either as a conformational switch modulating the multiple target repertory of E7 or in redox catalysis protecting C24 from oxidation in an oxidized milieu, requires further research. In both scenarios, C59 could act as the reactive or catalytic cysteine and C68 as a resolving cysteine. Reversibility is strictly required to accomplish both regulatory and catalytic functions, a condition that is fulfilled by the redox behavior of the E7 HPV16 protein (Figure 7). Additionally, sequence analysis shows that virtually all E7 proteins presenting at least two noncanonical cysteines possess one cysteine in Cluster 1, a cluster likely to harbor exposed and highly reactive cysteines.[25] In line with this, some peroxiredoxins (1-Cys) lack the resolving cysteine, which is substituted by low molecular weight thiols, but the absence of a catalytic cysteine is irreplaceable for redox activity.[68]

A possible direct function for a redox catalytic pair in E7 could involve maintaining C24 in a reduced state, allowing Rb binding despite the presence of the oxidative environment observed in HPV-transformed tissues. In support of this, our results show that the full length E7 protein partially protects C24 from glutathionylation (Figure 3). Recently, it has been reported that the Glutathione S-transferase P1 (GST-P1) protein is also a target of HPV16 E7 protein.[19] E7 binds to GST-P1 through a region that comprises amino acids 40−60 of the E7 sequence, and the E7-GSTP1 interaction modifies the redox equilibrium between the reduced and oxidized GST-P1 protein in favor of the reduced state of the enzyme.[19] The reduced GST-P1 interacts and inhibits the c-Jun N-terminal kinase (JNK), which in turn is unable to phosphorylate the Jun protein. Since JNK-mediated signal transduction leads to apoptosis, it has been suggested that this is the mechanism by which HPV16 E7 transformed keratinocytes escape apoptosis.

The presence of noncanonical cysteines in 70% of E7 sequences including most clinically relevant HPV strains suggests that redox regulation may be a common property shared by a large number of E7 proteins, and the study of redox mechanisms is of particular interest in high-risk E7 proteins, known to be constitutively expressed in an oxidative environment within HPV-transformed cells. Finally, the multiple reported cellular effects of E7 could well be related to moonlighting functions that are redox-regulated. In this scenario, redox regulation provides an additional layer of conformational diversity to E7, allowing this small multitarget viral protein to gain complexity without paying the cost of an enlarged viral genome size.

■ ASSOCIATED CONTENT

Supporting Information

Supplementary Figures S1−S4 and Supplementary Table 1. This material is available free of charge via the Internet at http://pubs.acs.org.

■ AUTHOR INFORMATION

Corresponding Authors

*Ph: +54 11 52387500. E-mail: gpg@leloir.org.ar.
*Ph: +54 11 52387500. E-mail: lalonso@leloir.org.ar.

Author Contributions

§These authors contributed equally to this work.

Funding

This work was supported by a Grant for Basic Research from Instituto Nacional del Cáncer (National Health Ministry, Argentina). All authors are career investigators from Consejo Nacional de Investigaciones Científicas y Técnicas (CONICET, Science and Technology Ministry, Argentina).

Notes

The authors declare no competing financial interest.

■ ABBREVIATIONS

HPV, human papillomavirus; Rb, retinoblastoma protein; IDD, intrinsically disordered domain; E7SOs, E7 spherical soluble oligomers; DTT, dithiothreitol; PMPS, *p*-hydroxymercuriphenylsulfonate; PAR, 4-(2-pyridylazo) resorcinol; DTNB, 5,5′-dithiobis(2-nitrobenzoic acid); GSH, reduced glutathione; GSSG, oxidized glutathione; RP-HPLC, reverse-phase high-performance liquid chromatography; IAA, iodoacetamide; NEM, *N*-ethylmaleimide; CD, circular dichroism; GdmCl, guanidinium chloride; TFA, trifluoroacetic acid; OPG, octyl β-D-glucopyranoside; HCCA, α-cyano-4-hydroxycinnamic acid

■ REFERENCES

(1) zur Hausen, H. (1996) Papillomavirus infections—a major cause of human cancers. *Biochim. Biophys. Acta 1288*, F55−78.

(2) Munoz, N., Bosch, F. X., de Sanjose, S., Herrero, R., Castellsague, X., Shah, K. V., Snijders, P. J., and Meijer, C. J. (2003) Epidemiologic classification of human papillomavirus types associated with cervical cancer. *N. Engl. J. Med. 348*, 518−527.

(3) Bernard, H. U., Burk, R. D., Chen, Z., van Doorslaer, K., zur Hausen, H., and de Villiers, E. M. (2010) Classification of papillomaviruses (PVs) based on 189 PV types and proposal of taxonomic amendments. *Virology 401*, 70−79.

(4) Schiffman, M., Herrero, R., Desalle, R., Hildesheim, A., Wacholder, S., Rodriguez, A. C., Bratti, M. C., Sherman, M. E., Morales, J., Guillen, D., Alfaro, M., Hutchinson, M., Wright, T. C., Solomon, D., Chen, Z., Schussler, J., Castle, P. E., and Burk, R. D. (2005) The carcinogenicity of human papillomavirus types reflects viral evolution. *Virology 337*, 76−84.

(5) Doorbar, J. (2005) The papillomavirus life cycle. *J. Clin. Virol. 32* (Suppl 1), S7−15.

(6) Howley, P. M. (1996) *Fields Virology*, 3rd ed., Raven Publishers, Philadelphia.

(7) Helt, A. M., Funk, J. O., and Galloway, D. A. (2002) Inactivation of both the retinoblastoma tumor suppressor and p21 by the human papillomavirus type 16 E7 oncoprotein is necessary to inhibit cell cycle arrest in human epithelial cells. *J. Virol. 76*, 10559−10568.

(8) Banerjee, N. S., Genovese, N. J., Noya, F., Chien, W. M., Broker, T. R., and Chow, L. T. (2006) Conditionally activated E7 proteins of high-risk and low-risk human papillomaviruses induce S phase in postmitotic, differentiated human keratinocytes. *J. Virol. 80*, 6517−6524.

(9) Moody, C. A., and Laimins, L. A. (2010) Human papillomavirus oncoproteins: pathways to transformation. *Nat. Rev. Cancer 10*, 550−560.

(10) Pim, D., and Banks, L. (2010) Interaction of viral oncoproteins with cellular target molecules: infection with high-risk vs low-risk human papillomaviruses. *APMIS 118*, 471−493.

(11) Dyson, N., Howley, P. M., Munger, K., and Harlow, E. (1989) The human papilloma virus-16 E7 oncoprotein is able to bind to the retinoblastoma gene product. *Science 243*, 934−937.

(12) Munger, K., and Howley, P. M. (2002) Human papillomavirus immortalization and transformation functions. *Virus Res 89*, 213−228.
(13) Munger, K., Werness, B. A., Dyson, N., Phelps, W. C., Harlow, E., and Howley, P. M. (1989) Complex formation of human papillomavirus E7 proteins with the retinoblastoma tumor suppressor gene product. *EMBO J. 8*, 4099−4105.
(14) Heck, D. V., Yee, C. L., Howley, P. M., and Munger, K. (1992) Efficiency of binding the retinoblastoma protein correlates with the transforming capacity of the E7 oncoproteins of the human papillomaviruses. *Proc. Natl. Acad. Sci. U.S.A. 89*, 4442−4446.
(15) Crook, T., Morgenstern, J. P., Crawford, L., and Banks, L. (1989) Continued expression of HPV-16 E7 protein is required for maintenance of the transformed phenotype of cells co-transformed by HPV-16 plus EJ-ras. *EMBO J. 8*, 513−519.
(16) De Marco, F., Bucaj, E., Foppoli, C., Fiorini, A., Blarzino, C., Filipi, K., Giorgi, A., Schinina, M. E., Di Domenico, F., Coccia, R., Butterfield, D. A., and Perluigi, M. (2012) Oxidative stress in HPV-driven viral carcinogenesis: redox proteomics analysis of HPV-16 dysplastic and neoplastic tissues. *PLoS One 7*, e34366.
(17) De Marco, F. (2013) Oxidative stress and HPV carcinogenesis. *Viruses 5*, 708−731.
(18) Williams, V. M., Filippova, M., Soto, U., and Duerksen-Hughes, P. J. (2011) HPV-DNA integration and carcinogenesis: putative roles for inflammation and oxidative stress. *Future Virol. 6*, 45−57.
(19) Mileo, A. M., Abbruzzese, C., Mattarocci, S., Bellacchio, E., Pisano, P., Federico, A., Maresca, V., Picardo, M., Giorgi, A., Maras, B., Schinina, M. E., and Paggi, M. G. (2009) Human papillomavirus-16 E7 interacts with glutathione S-transferase P1 and enhances its role in cell survival. *PLoS One 4*, e7254.
(20) Alonso, L. G., Garcia-Alai, M. M., Nadra, A. D., Lapena, A. N., Almeida, F. L., Gualfetti, P., and Prat-Gay, G. D. (2002) High-risk (HPV16) human papillomavirus E7 oncoprotein is highly stable and extended, with conformational transitions that could explain its multiple cellular binding partners. *Biochemistry 41*, 10510−10518.
(21) Ohlenschlager, O., Seiboth, T., Zengerling, H., Briese, L., Marchanka, A., Ramachandran, R., Baum, M., Korbas, M., Meyer-Klaucke, W., Durst, M., and Gorlach, M. (2006) Solution structure of the partially folded high-risk human papilloma virus 45 oncoprotein E7. *Oncogene 25*, 5953−5959.
(22) Liu, X., Clements, A., Zhao, K., and Marmorstein, R. (2006) Structure of the human Papillomavirus E7 oncoprotein and its mechanism for inactivation of the retinoblastoma tumor suppressor. *J. Biol. Chem. 281*, 578−586.
(23) Garcia-Alai, M. M., Alonso, L. G., and de Prat-Gay, G. (2007) The N-terminal module of HPV16 E7 is an intrinsically disordered domain that confers conformational and recognition plasticity to the oncoprotein. *Biochemistry 46*, 10405−10412.
(24) Clements, A., Johnston, K., Mazzarelli, J. M., Ricciardi, R. P., and Marmorstein, R. (2000) Oligomerization properties of the viral oncoproteins adenovirus E1A and human papillomavirus E7 and their complexes with the retinoblastoma protein. *Biochemistry 39*, 16033−16045.
(25) Chemes, L. B., Glavina, J., Alonso, L. G., Marino-Buslje, C., de Prat-Gay, G., and Sanchez, I. E. (2012) Sequence evolution of the intrinsically disordered and globular domains of a model viral oncoprotein. *PLoS One 7*, No. e47661.
(26) McIntyre, M. C., Frattini, M. G., Grossman, S. R., and Laimins, L. A. (1993) Human papillomavirus type 18 E7 protein requires intact Cys-X-X-Cys motifs for zinc binding, dimerization, and transformation but not for Rb binding. *J. Virol. 67*, 3142−3150.
(27) Alonso, L. G., Garcia-Alai, M. M., Smal, C., Centeno, J. M., Iacono, R., Castano, E., Gualfetti, P., and de Prat-Gay, G. (2004) The HPV16 E7 viral oncoprotein self-assembles into defined spherical oligomers. *Biochemistry 43*, 3310−3317.
(28) Patrick, D. R., Oliff, A., and Heimbrook, D. C. (1994) Identification of a novel retinoblastoma gene product binding site on human papillomavirus type 16 E7 protein. *J. Biol. Chem. 269*, 6842−6850.
(29) Miseta, A., and Csutora, P. (2000) Relationship between the occurrence of cysteine in proteins and the complexity of organisms. *Mol. Biol. Evol. 17*, 1232−1239.
(30) World Health Organization International Agency for Research on Cancer (1995) Human papillomavirus. *IARC Monographs on the Evaluation of Carcinogenic Risks to Humans*, Vol. *64*, pp 1−409, World Health Organization, Geneva.
(31) Marino, S. M., and Gladyshev, V. N. (2010) Cysteine function governs its conservation and degeneration and restricts its utilization on protein surfaces. *J. Mol. Biol. 404*, 902−916.
(32) Ferrer-Sueta, G., Manta, B., Botti, H., Radi, R., Trujillo, M., and Denicola, A. (2011) Factors affecting protein thiol reactivity and specificity in peroxide reduction. *Chem. Res. Toxicol. 24*, 434−450.
(33) Pace, N. J., and Weerapana, E. (2013) Diverse functional roles of reactive cysteines. *ACS Chem. Biol. 8*, 283−296.
(34) Thamsen, M., and Jakob, U. (2011) The redoxome: Proteomic analysis of cellular redox networks. *Curr. Opin. Chem. Biol. 15*, 113−119.
(35) Reddie, K. G., and Carroll, K. S. (2008) Expanding the functional diversity of proteins through cysteine oxidation. *Curr. Opin. Chem. Biol. 12*, 746−754.
(36) Pimentel, D., Haeussler, D. J., Matsui, R., Burgoyne, J. R., Cohen, R. A., and Bachschmid, M. M. (2012) Regulation of cell physiology and pathology by protein S-glutathionylation: lessons learned from the cardiovascular system. *Antioxid. Redox Signal. 16*, 524−542.
(37) Anathy, V., Roberson, E. C., Guala, A. S., Godburn, K. E., Budd, R. C., and Janssen-Heininger, Y. M. (2012) Redox-based regulation of apoptosis: S-glutathionylation as a regulatory mechanism to control cell death. *Antioxid. Redox Signal. 16*, 496−505.
(38) Tanner, J. J., Parsons, Z. D., Cummings, A. H., Zhou, H., and Gates, K. S. (2011) Redox regulation of protein tyrosine phosphatases: structural and chemical aspects. *Antioxid. Redox Signal. 15*, 77−97.
(39) Neumann, C. A., Cao, J., and Manevich, Y. (2009) Peroxiredoxin 1 and its role in cell signaling. *Cell Cycle 8*, 4072−4078.
(40) Bulaj, G., Kortemme, T., and Goldenberg, D. P. (1998) Ionization-reactivity relationships for cysteine thiols in polypeptides. *Biochemistry 37*, 8965−8972.
(41) Gilbert, H. F. (1995) Thiol/disulfide exchange equilibria and disulfide bond stability. *Methods Enzymol. 251*, 8−28.
(42) Laemmli, U. K. (1970) Cleavage of structural proteins during the assembly of the head of bacteriophage. *Nature 227*, 680−685.
(43) Hunt, J. B., Neece, S. H., and Ginsburg, A. (1985) The use of 4-(2-pyridylazo)resorcinol in studies of zinc release from Escherichia coli aspartate transcarbamoylase. *Anal. Biochem. 146*, 150−157.
(44) Ellman, G., and Lysko, H. (1979) A precise method for the determination of whole blood and plasma sulfhydryl groups. *Anal. Biochem. 93*, 98−102.
(45) Chemes, L. B., Sanchez, I. E., Smal, C., and de Prat-Gay, G. (2010) Targeting mechanism of the retinoblastoma tumor suppressor by a prototypical viral oncoprotein. Structural modularity, intrinsic disorder and phosphorylation of human papillomavirus E7. *FEBS J. 277*, 973−988.
(46) Edgar, R. C. (2004) MUSCLE: multiple sequence alignment with high accuracy and high throughput. *Nucleic Acids Res. 32*, 1792−1797.
(47) Sali, A., and Blundell, T. L. (1993) Comparative protein modelling by satisfaction of spatial restraints. *J. Mol. Biol. 234*, 779−815.
(48) Eswar, N., Webb, B., Marti-Renom, M. A., Madhusudhan, M. S., Eramian, D., Shen, M. Y., Pieper, U., and Sali, A. (2006) Comparative protein structure modeling using Modeller, in *Current Protocols in Bioinformatics* (Baxevanis, D., et al., Eds.) Chapter 5, Unit 5.6, Wiley, New York.
(49) Kabsch, W., and Sander, C. (1983) Dictionary of protein secondary structure: pattern recognition of hydrogen-bonded and geometrical features. *Biopolymers 22*, 2577−2637.
(50) Morgan, B., Ezerina, D., Amoako, T. N., Riemer, J., Seedorf, M., and Dick, T. P. (2013) Multiple glutathione disulfide removal pathways mediate cytosolic redox homeostasis. *Nat. Chem. Biol. 9*, 119−125.
(51) Veal, E. A., Day, A. M., and Morgan, B. A. (2007) Hydrogen peroxide sensing and signaling. *Mol. Cell 26*, 1−14.

(52) Stadtman, E. R., and Berlett, B. S. (1998) Reactive oxygen-mediated protein oxidation in aging and disease. *Drug Metab. Rev. 30*, 225−243.
(53) Chemes, L. B., Sanchez, I. E., and de Prat-Gay, G. (2011) Kinetic recognition of the retinoblastoma tumor suppressor by a specific protein target. *J. Mol. Biol. 412*, 267−284.
(54) Shevchenko, A., Tomas, H., Havlis, J., Olsen, J. V., and Mann, M. (2006) In-gel digestion for mass spectrometric characterization of proteins and proteomes. *Nat. Protoc. 1*, 2856−2860.
(55) Phelps, W. C., Munger, K., Yee, C. L., Barnes, J. A., and Howley, P. M. (1992) Structure-function analysis of the human papillomavirus type 16 E7 oncoprotein. *J. Virol. 66*, 2418−2427.
(56) Todorovic, B., Massimi, P., Hung, K., Shaw, G. S., Banks, L., and Mymryk, J. S. (2011) Systematic analysis of the amino acid residues of human papillomavirus type 16 E7 conserved region 3 involved in dimerization and transformation. *J. Virol. 85*, 10048−10057.
(57) Dong, W. L., Caldeira, S., Sehr, P., Pawlita, M., and Tommasino, M. (2001) Determination of the binding affinity of different human papillomavirus E7 proteins for the tumour suppressor pRb by a plate-binding assay. *J. Virol. Methods 98*, 91−98.
(58) Ruden, D. M., Garfinkel, M. D., Sollars, V. E., and Lu, X. (2003) Waddington's widget: Hsp90 and the inheritance of acquired characters. *Sem. Cell Dev. Biol. 14*, 301−310.
(59) Jakob, U., Eser, M., and Bardwell, J. C. (2000) Redox switch of hsp33 has a novel zinc-binding motif. *J. Biol. Chem. 275*, 38302−38310.
(60) Jakob, U., Muse, W., Eser, M., and Bardwell, J. C. (1999) Chaperone activity with a redox switch. *Cell 96*, 341−352.
(61) Bourles, E., Isaac, M., Lebrun, C., Latour, J. M., and Seneque, O. (2011) Oxidation of Zn(Cys)4 zinc finger peptides by O2 and H2O2: products, mechanism and kinetics. *Chemistry 17*, 13762−13772.
(62) Christman, M. F., Storz, G., and Ames, B. N. (1989) OxyR, a positive regulator of hydrogen peroxide-inducible genes in Escherichia coli and Salmonella typhimurium, is homologous to a family of bacterial regulatory proteins. *Proc. Natl. Acad. Sci. U.S.A. 86*, 3484−3488.
(63) Choi, H., Kim, S., Mukhopadhyay, P., Cho, S., Woo, J., Storz, G., and Ryu, S. E. (2001) Structural basis of the redox switch in the OxyR transcription factor. *Cell 105*, 103−113.
(64) Littler, D. R., Harrop, S. J., Fairlie, W. D., Brown, L. J., Pankhurst, G. J., Pankhurst, S., DeMaere, M. Z., Campbell, T. J., Bauskin, A. R., Tonini, R., Mazzanti, M., Breit, S. N., and Curmi, P. M. (2004) The intracellular chloride ion channel protein CLIC1 undergoes a redox-controlled structural transition. *J. Biol. Chem. 279*, 9298−9305.
(65) Marino, S. M., and Gladyshev, V. N. (2012) Analysis and functional prediction of reactive cysteine residues. *J. Biol. Chem. 287*, 4419−4425.
(66) Choi, J., Choi, S., Choi, J., Cha, M. K., Kim, I. H., and Shin, W. (2003) Crystal structure of Escherichia coli thiol peroxidase in the oxidized state: insights into intramolecular disulfide formation and substrate binding in atypical 2-Cys peroxiredoxins. *J. Biol. Chem. 278*, 49478−49486.
(67) Hall, A., Nelson, K., Poole, L. B., and Karplus, P. A. (2011) Structure-based insights into the catalytic power and conformational dexterity of peroxiredoxins. *Antioxid. Redox Signal. 15*, 795−815.
(68) Fomenko, D. E., and Gladyshev, V. N. (2003) Identity and functions of CxxC-derived motifs. *Biochemistry 42*, 11214−11225.